UNIVERSITÀ
DEGLI STUDI
FIRENZE

DOTTORATO DI RICERCA IN SCIENZE CHIMICHE

CICLO XXXII

COORDINATORE Prof. PIERO BAGLIONI

DEVELOPMENT AND CHARACTERIZATION OF GREEN LIPID-BASED NANOVECTORS FOR AGRICULTURAL APPLICATIONS

SVILUPPO E CARATTERIZZAZIONE DI NANOVETTORI LIPIDICI "VERDI" PER APPLICAZIONI AGRONOMICHE

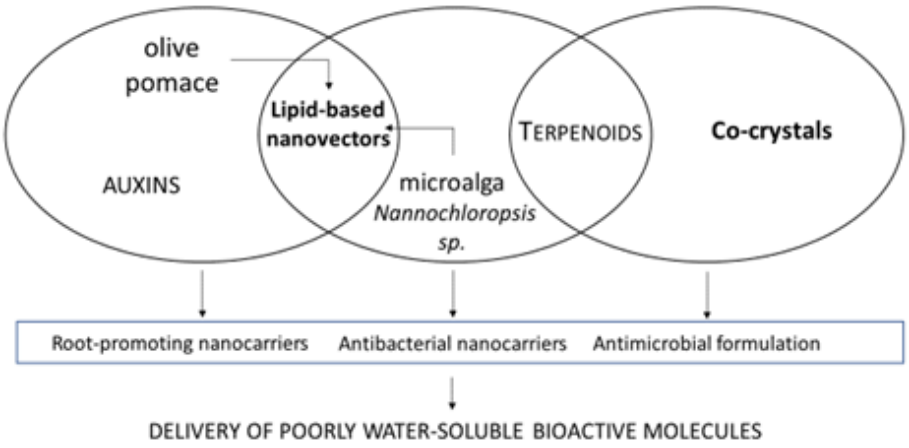

Dottorando
Dott. Felicia Menicucci

Tutore
Prof. Sandra Ristori

UNIVERSITÀ
DEGLI STUDI
FIRENZE

DOTTORATO DI RICERCA IN SCIENZE CHIMICHE

CICLO XXXII

COORDINATORE Prof. BAGLIONI PIERO

DEVELOPMENT AND CHARACTERIZATION OF GREEN LIPID-BASED NANOVECTORS FOR AGRICULTURAL APPLICATIONS

Settore Scientifico Disciplinare CHIM/02

Dottorando
Dott. *Menicucci Felicia*

_____

(firma)

Tutore
Prof. *Ristori Sandra*

_____

(firma)

Coordinatore
Prof. *Baglioni Piero*

_____

(firma)

Anni 2016/2019

INDEX

RIASSUNTO

L'impiego di ingenti quantitativi di antiparassitari, diserbanti ed altri prodotti chimici di sintesi ha fortemente compromesso la qualità dei raccolti e la produttività dei terreni agricoli, con serie ripercussioni sull'ambiente e sulla salute dell'uomo e degli animali. In Europa una maggior sensibilità dell'opinione pubblica verso questo tipo di tematiche e l'urgenza di trovare valide alternative ai metodi più comunemente utilizzati, hanno richiamato l'attenzione di molti dei paesi membri, che da alcuni anni stanno proponendo politiche ambientali più sostenibili. In questo contesto, le nanotecnologie rappresentano uno strumento di supporto utile allo sviluppo di nuove strategie e metodologie di trattamento in ambito agronomico. Nella presente tesi di dottorato sono state affrontate due problematiche di interesse primario per questo settore, vale a dire produttività e impiego di antiparassitari. A tal fine sono stati realizzati dei nanovettori lipidici utilizzando biorisorse naturali, con l'obiettivo ultimo di promuovere l'efficacia delle molecole veicolate dal nanosistema stesso. La scelta di utilizzare questo tipo di nanotecnologia nasce dai numerosi vantaggi d'impiego dei nanovettori a base lipidica, la cui composizione li rende particolarmente biocompatibili e biodegradabili. Nel primo caso è stato ideato e sviluppato un formulato per il trasporto di auxine derivato da uno scarto del processo di spremitura delle olive, la sansa di oliva. Le auxine sono ormoni vegetali comunemente utilizzati in floricoltura e nella riproduzione per talea per promuovere lo sviluppo e l'accrescimento della pianta. La scarsa idrosolubilità di questi composti, tuttavia, ne limita la biodisponibilità e, di conseguenza, l'efficacia di azione. Questo inconveniente è stato aggirato caricando le auxine nei nanovettori

lipidici ottenuti da sansa di oliva, la cui struttura è stata caratterizzata tramite tecniche di Dynamic Light Scattering, potenziale zeta e Small-angle X-ray Scattering e la cui efficacia è stata infine testata su talee di olivo appartenenti a tre differenti cultivar. I risultati ottenuti hanno mostrato un aumento della percentuale di radicazione rispetto ai trattamenti convenzionali in due delle tre cultivar selezionate. Nel secondo caso *Nannochloropsis* sp., una microalga marina principalmente costituita di lipidi, è stata scelta come biorisorsa per la realizzazione di nanovettori caricati con timolo. Questo terpenoide si ritrova nella miscela aromatica di numerose specie vegetali ed è un potente antibatterico e fungicida naturale. La sua natura volatile, però, ne pregiudica l'efficacia a lungo termine, limitandone fortemente le potenzialità. In questo lavoro il carattere idrofobico di questa molecola è stato sfruttato per favorirne l'associazione con i nanovettori lipidici ottenuti da alga che, fungendo da veri e propri siti di accumulo, sono stati sperimentati come agenti di trasporto dell'antibatterico in esperimenti *in vitro* condotti contro un batterio patogeno della pianta di pomodoro. I risultati di questi test hanno mostrato una completa inibizione della crescita batterica in presenza di nanovettori carichi di timolo per concentrazioni pari o superiori a 250 ppm. Struttura e dimensioni dei nanovettori sono state determinate tramite le tecniche sopracitate e il dosaggio del timolo caricato al loro interno è stato ottenuto mediante gas-cromatografia accoppiata a spettrometria di massa. Infine, l'utilizzo di timolo, carvacrolo ed eugenolo come antimicrobici naturali è stato ulteriormente indagato sperimentando l'efficacia di una formulazione solida, alternativa ai nanovettori lipidici in solvente acquoso. Questi tre terpenoidi sono stati scelti per lo sviluppo di sei co-cristalli, combinando ciascuno di essi con fenazina o esametilentetrammina (coformeri) secondo un

preciso rapporto stechiometrico; in tal modo sono stati ottenuti dei formulati di natura polverulenta la cui bioattività è stata saggiata *in vitro* contro sei specie batteriche e tre fungine fitopatogene o benefiche per le piante. I risultati ottenuti hanno mostrato come l'efficacia dei monoterpeni venga in alcuni casi potenziata dalla combinazione con il coformero, poiché a parità di concentrazione, alcuni co-cristalli mostrano un'azione biocida significativamente superiore a quella dei corrispondenti costituenti puri. Il rilascio della molecola bioattiva dal co-cristallo è stato inoltre studiato nel tempo a differenti temperature tramite gas-cromatografia accoppiata a spettrometria di massa in modalità spazio di testa. Il profilo di rilascio relativo al co-cristallo è risultato significativamente diverso rispetto a quello del composto puro, mettendo in risalto il ruolo chiave giocato dal processo di co-cristallizzazione nel promuovere un rilascio più controllato e protratto nel tempo della molecola bioattiva, garantendone quindi un'efficacia d'azione più prolungata. In conclusione, in questa tesi vengono presentate tre formulazioni a base di composti derivati dalle piante, di cui due in solvente acquoso e una allo stato solido; la loro efficacia è stata studiata tramite test di laboratorio con l'intento finale di ideare e realizzare prodotti alternativi ai fitofarmaci tradizionali per possibili impieghi in agricoltura.

PREFACE

Nanotechnologies include a wide range of devices of nanometer scale size, which find application in many different fields, such as medicine, aerospace, energy production and agriculture, to name but a few[1,2]. Dealing with biomedical applications, nano-emulsions, dendrimers, nano-gold shells, magnetic nanoparticles and liposomes, are only some examples of the currently available nanotechnology platforms. Among these, lipid-based nanoparticles have been the longest-studied nanocarriers, due to the fact that they are the least toxic for *in vivo* applications[3]. Their lipid composition improves biodegradability, biocompatibility, as well as their effectiveness as drug-delivery systems able to easily transport the payload across biological membranes. In addition, thanks to their hydrophobic structure, lipid carriers may allow the delivery of slightly water-soluble drugs and prevent drug degradation, acting as protective vehicles.

Among different families of lipid-based nanoparticles, particular attention has been paid to liposomes and solid lipid nanoparticles (SLNs) (Fig.1), together with nanostructured lipid carriers (NLCs), which are considered the second generation of SLNs[4].

Being the most studied and the first to be developed in the early 60s of the last century, liposomes represent a milestone in the history of lipid-based nanocarriers. Their structure consists of a lipid bilayer of amphiphilic phospholipids enclosing an aqueous core, where hydrophilic drugs can be entrapped to be delivered. At the same time, the hydrophobic fatty acid chains of the phospholipids represent a suitable environment to store

lipophilic drugs, making liposomes a versatile nanoplatform for the inclusion of both lipophilic and hydrophilic compounds[3,5,6].

SLNs and NLCs were developed more recently. They are both characterized by a hydrophobic core that may be composed of glycerides, fatty acids, steroids and waxes, which perfectly meets the requirements for lipophilic drugs' loading. Since their synthesis can be solvent-free, as well as implying low cost processes, this typology of lipid carriers has gained noteworthy interest, especially concerning scale-up production[3,4].

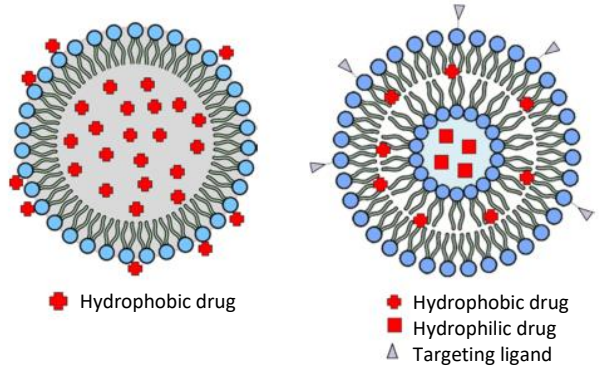

Figure 1. Schematic representation of a solid lipid nanoparticle (left) and of a liposome (right). Picture from García et Al. (2018). Self-assembled nanomaterials; *Nanobiomaterials*.

The employment of nanotechnology in agriculture is relatively new, especially dealing with plant protection and production[7]. Since a transition from an intensive farming based on the massive use of pesticides and conventional phytochemicals towards a more sustainable one is by now mandatory[8], the development of alternative formulations has been investigated in this work. Specifically, two natural matrixes were used as source of physiological lipids for the fabrication of nanoparticles, which were loaded with plant-derived compounds. The design, the structural characterization and finally, the testing

of these nanovectors, are presented and discussed in the first and second section of this thesis.

Moreover, a formulation of co-crystals mainly composed of natural constituents was provided by the Department of Chemistry, Life Sciences and Environmental Sustainability of the University of Parma and tested as antimicrobial. Results of this experimentation are shown in the last section of the thesis.

Contents

A brief description of the work carried out during this PhD follows below and the setting of the thesis is graphically summarized in figure 2.

In the first section, a specifically designed methodology for phytohormones' application on olive cuttings is presented and experimented. More in depth, olive pomace was employed as lipid source for the development of nanocarriers delivering auxins as root-promoting phytohormones. Auxins are poorly soluble in water, thus lipid nanovectors were fabricated as carriers for their delivering to the roots, in order to improve their plant availability. In addition, the biocompatibility of these devices was improved choosing olive pomace as raw material for the manufacturing, and olive cuttings as final target of the experimentation, originating a green circle starting from olive waste and ending with olive plant itself.

The second part of this thesis deals with the development of lipid-based nanocarriers derived from the microalga *Nannochloropsis sp*.

Similarly to auxins' carrier-mediated transport, the obtained nanodevices were used to overcome the poor water solubility of the bioactive molecule to be delivered, thymol, and also to reduce its volatilization. This terpenoid belongs to a large family of plant-derived compounds which has received remarkable attention because of the peculiar characteristics displayed as antimicrobial, antifungal, insecticidal and antioxidant natural agents[9]. An evaluation of the antibacterial activity of the thymol-delivering nanovectors was carried out against a gram-negative bacterium affecting tomato and pepper plants.

Finally, the third section is dedicated to a project in collaboration with the Department of Chemistry, Life Sciences and Environmental Sustainability of the University of Parma, where a powdery formulation of co-crystals specifically designed for the delivery of terpenoids was developed. A set of six co-crystals was synthesized matching thymol, eugenol and carvacrol with hexamethylenetetramine and phenazine in a specific stoichiometric ratio.
The release profile of the bioactive molecules from the co-crystals were determined and the antibacterial and fungicidal activity displayed by this formulation was studied *in vitro* against six bacterial and three fungi species.

Despite the different composition, state of matter and final purpose of use, all the systems studied during this PhD were specifically designed to favor the association with the compounds to be loaded, in order to overcome the poor water solubility displayed by auxins and terpenoids. The molecules selected for the delivery were all plant-derived and the composition of the three formulations was primarily based on the employment of natural constituents

extracted, purified or recovered by biological matrixes, being one of the prime intents that of proposing a biocompatible and low-toxic alternative to the conventional phytochemicals.

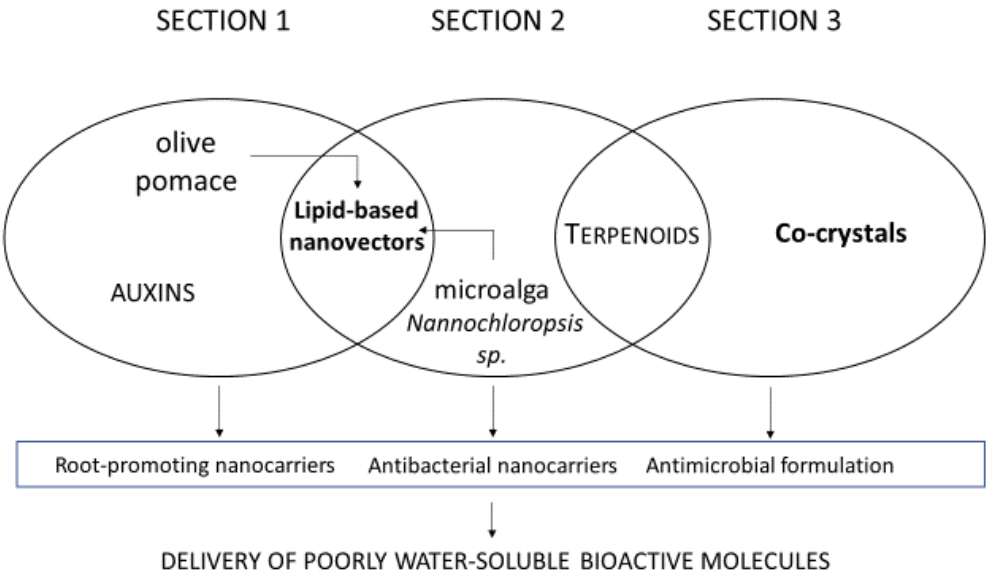

Figure 2. Graphic summary of the thesis, organized in three sections.

REFERENCES

[1] García, M. C., Aloisio, C., Onnainty, R., & Ullio-Gamboa, G. (2018). Self-assembled nanomaterials. In Nanobiomaterials (pp. 41-94). Woodhead Publishing.

[2] Prasad, R., Kumar, V., & Prasad, K. S. (2014). Nanotechnology in sustainable agriculture: present concerns and future aspects. African Journal of Biotechnology, 13(6), 705-713.

[3] Puri, A., Loomis, K., Smith, B., Lee, J. H., Yavlovich, A., Heldman, E., & Blumenthal, R. (2009). Lipid-based nanoparticles as pharmaceutical drug carriers: from concepts to clinic. Critical Reviews™ in Therapeutic Drug Carrier Systems, 26(6).

[4] Campani, V., Giarra, S., & De Rosa, G. (2018). Lipid-based core-shell nanoparticles: Evolution and potentialities in drug delivery. OpenNano, 3, 5-17.

[5] Madni, A., Sarfraz, M., Rehman, M., Ahmad, M., Akhtar, N., Ahmad, S., ... & Löbenberg, R. (2014). Liposomal drug delivery: a versatile platform for challenging clinical applications. Journal of Pharmacy & Pharmaceutical Sciences, 17(3), 401-426.

[6] Pattni, B. S., Chupin, V. V., & Torchilin, V. P. (2015). New developments in liposomal drug delivery. Chemical reviews, 115(19), 10938-10966.

[7] Khot, L. R., Sankaran, S., Maja, J. M., Ehsani, R., & Schuster, E. W. (2012). Applications of nanomaterials in agricultural production and crop protection: a review. Crop protection, 35, 64-70.

[8] Hossain, L., Rahman, R., & Khan, M. S. (2017). Alternatives of pesticides. In Pesticide residue in foods (pp. 147-165). Springer, Cham.

[9] Elshafie, H. S., Gruľová, D., Baranová, B., Caputo, L., De Martino, L., Sedlák, V., ... & De Feo, V. (2019). Antimicrobial activity and chemical composition of essential oil extracted from Solidago canadensis L. growing wild in Slovakia. Molecules, 24(7), 1206.

SECTION 1. OLIVE POMACE-DERIVED NANOVECTORS FOR THE DELIVERY OF AUXINS

1.1 INTRODUCTION

During the last decades, the massive use of pesticides and agrochemicals has caused serious damages to the ecosystem, leading to soil degradation, environmental pollution and development of resistant plant pathogens. Therefore, sustainable and eco-friendlier technologies to increase both quantity and quality of agricultural products are by now needed[1].

In this context, new plant biotechnologies at the nanoscale level have proved to be useful tools to manage some challenges in agricultural sciences[2,3]. Phytochemical drugs can be encapsulated within inorganic nanoparticles (i.e. obtained from metal or metal oxides) or in soft matter nanocarriers: both these vectors can allow micro-transportation and intracellular delivery of poorly water-soluble molecules[4,5].

Lipid-based nanocarriers, such as liposomes and micelles, have been largely used as delivery systems as well as for imaging purposes in the biomedical field[6].

Their employment could be extended to agriculture, designing suitable nanovectors able to interact with plant cell membranes, taking advantage of the superior biocompatibility displayed by lipid-based nanocarriers. Using lipid mixtures extracted from the target organisms themselves is an innovative procedure in drug delivery that may facilitate the carrier-target interaction, and consequently, improve the effectiveness of encapsulated drugs.

In line with the philosophy of a sustainable approach inspired by green chemistry principles, lipids to fabricate nanocarriers can be obtained from microorganisms or from plants. In order to make the process not only eco-friendly, but also helpful for the circular economy, it is desirable to re-utilize waste-products difficult to eliminate, such as olive mill pomace (OMP), as sources of lipids[7]. The OMP is the solid waste made up of small pieces of stone and parts of the olive pulp and skin.

It is produced in large quantities from the olive oil industry and it is potentially harmful if freely discarded in the environment, because of its low pH, high salinity and presence of phytotoxic substances[7].

Nanotechnologies could open up new opportunities in agriculture, especially for one of its most limiting factors, that is a sustainable vegetative propagation of plants[2]. *In vivo* and *in vitro* vegetative propagation is necessary to produce clones, individuals genetically equal to each other and to the mother plant. Vegetative propagation allows to obtain healthier crops with specific agronomical and morphological traits of interest. Concerning plant multiplication, the most widely used root promoting compounds are auxins (mainly IAA, indole-3-acetic acid, IBA, indole-3-butyric acid, and NAA, 1-naphtaleneacetic acid), a class of molecules that can either be found in nature or synthesized[8]. Despite the help provided by phytohormone administration, the rooting process may be quite difficult in greenhouses, and this is not only due to the intrinsically different root ability of the cultivated varieties, but also to the poor auxins' solubility in water media. This inconvenient negatively affects auxins' transport from the site of application to the root initiation, thus reducing their availability[9]. To overcome these limitations, large amounts of growth regulators are used in conventional practices, but still many

horticultural and woody species remain recalcitrant to rooting[9]. Therefore, novel techniques for phytohormone administration should necessarily be aimed to increase their plant availability, decreasing the total amount of auxins employed at the same time.

In this project, olive pomace-derived nanovectors were developed and characterized in terms of structure and surface charge by physico-chemical techniques, such as Dynamic Light Scattering, Zeta Potential and Small Angle X-ray Scattering. Small amounts of purified phospholipids were also employed in the manufacturing, in order to improve the structure and shelf-stability of the carriers. Finally, an unconventional method of phytohormone administration was experimented on the initiation of the rooting process in *Olea europaea* L., an extensively cultivated species typical of the Mediterranean area. Specifically, three different cultivars were selected: "Canino" is a widespread cultivar in central Italy and was employed for *in vitro* experiments, whereas "Leccino" and "Leccio del Corno" were chosen for *in vivo* tests, the first being an easy-to-root and the latter a difficult-to-root cultivar.

1.2 MATERIALS AND METHODS

1.2.1 REAGENTS

1,2-Dioleyl-sn-glycero-3-phosphocholine (DOPC) and 1,2-dioleyl-sn-glycero-3-phosphoethanolamine (DOPE) were purchased from Lipoid GmbH. Indole-3-butyric acid (IBA) and 1-naphtaleneacetic acid (NAA), agar and all the components used in tissue culture were purchased from Sigma Aldrich.

1.2.2 FABRICATION OF NANOVECTORS

Olive pomace from various cultivars was provided by local oil producers, then mixed to obtain a homogeneous starting material, stored in freezer at -20 °C to prevent oxidation and de-frozen right before use. For lipid extraction, aliquots of 200 mg of olive pomace were treated with 1 mL Folch solution ($CHCl_3$:CH_3OH 2:1, v/v) under stirring at room temperature for 24 hours. Two types of systems were prepared: a) samples containing only lipids from pomace, b) samples containing lipids from olive pomace and pure phospholipids (DOPE or DOPC), added as adjuvant in small amount, i.e. 1:10 w/w with respect to the pomace. Consequently, by taking 50% as average lipid extraction, the final ratio was estimated to be 1:5 purified lipid: natural lipid. After solvent evaporation, a lipid film was obtained to which auxins dissolved in the proper organic solvents were added. Specifically, $CHCl_3$:C_3H_6O 2:1, v/v solution was used for IBA, while NAA was dissolved in $CHCl_3$. The stock concentration for both auxins was 10^{-2} M. Again, a dry lipid film was obtained by evaporation under-vacuum. This film was rehydrated with MilliQ water and equilibrated for 8-12 hours. The final suspension was homogenized through extensive vortexing, followed by eight cycles of freeze-thaw (i.e. soaking in liquid nitrogen, vortexing and then dipping samples in a warm bath at 45 °C). Subsequent sonication (5 cycles of 3 minutes each) at high power was used to downsize the lipid vectors. Noteworthy, this protocol allowed to scale the preparation up to a total volume of 1.2 L of lipid formulation in each trial. Smaller volumes (1-2 mL) for *in vitro* administration were prepared by extrusion performed 27 times with 100 nm polycarbonate porous membranes. These samples were filtered using sterile 0.45 µm pore filters and treated with UV light to avoid *in vitro* explant contamination during the

treatments. Sample names, composition, type of lipid used, and encapsulated auxin are summarized in table 1; molecular structures are also shown (Fig. 3).

Sample acronym	Composition	Lipid employed	Auxin loaded
E	200 mg/ml OP	Only OP lipids	empty
IBA	200 mg/ml OP + IBA 10-2 M	Only OP lipids	IBA
NAA	200 mg/ml OP + NAA 10-2 M	Only OP lipids	NAA
EPE	160 mg/ml OP + 20 mg/ml DOPE	OP lipids+ DOPE	empty
IPE	160 mg/ml OP + 20 mg/ml DOPE+ IBA 10-2 M	OP lipids+ DOPE	IBA
NPE	160 mg/ml OP + 20 mg/ml DOPE+ NAA 10-2 M	OP lipids+ DOPE	NAA
EPC	160 mg/ml OP + 20 mg/ml DOPC	OP lipids+ DOPC	empty
IPC	160 mg/ml OP + 20 mg/ml DOPC+ IBA 10-2 M	OP lipids+ DOPC	IBA
NPC	160 mg/ml OP + 20 mg/ml DOPC+ NAA 10-2 M	OP lipids+ DOPC	NAA

Table 1. Nomenclature and sample composition of olive pomace-derived nanovectors. DOPE=1,2-dioleyl-sn-glycero-3-phosphoethanolamine; DOPC=1,2-dioleyl-sn-glycero-3-phosphocholine; IBA=Indole-3-butyric acid; NAA=1-naphtaleneacetic acid; OP=olive pomace.

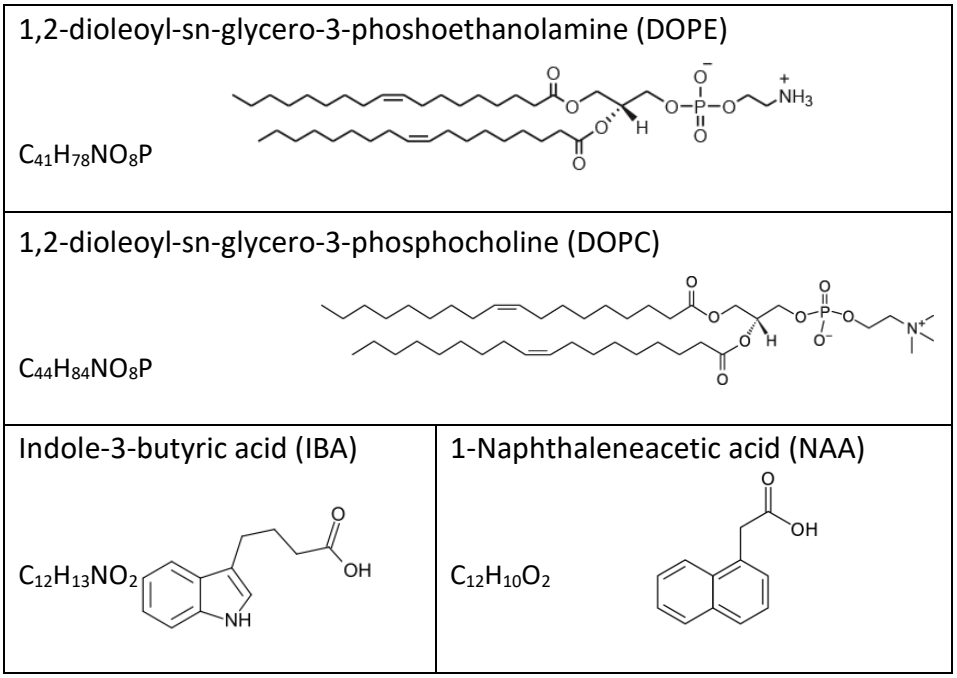

Figure 3. Molecule structures of auxins and phospholipids employed in nanovectors' fabrication.

1.2.3 NANOVECTORS' STRUCTURAL CHARACTERIZATION

DYNAMIC LIGHT SCATTERING AND ZETA POTENTIAL MEASUREMENTS

Dynamic Light Scattering (DLS), also known as Photon Correlation Spectroscopy, is a widely used technique to determine size, shape and size distribution of particles in suspension down to few nm of dimension. Briefly, a beam of monochromatic laser light is directed towards the cuvette holding the sample. The incoming light is deflected after hitting the diffusing particles: this corresponds to a changing of the scattered light wavelength that gives structural information about the distribution and dimensions of the scattering particles.

In this work, a Malvern Zetasizer (Nano ZS) instrument equipped with a He-Ne 633 nm, 4 mW laser with backscattering optics and micro-doppler effect analyzer for Zeta potential measures, was employed. Samples were diluted for 20 times with MilliQ water, to adjust the optical turbidity. The cumulant expansion was employed to analyze the autocorrelation function of the scattered intensity and to obtain mean size and polydispersity index (PdI)[10]. Data were acquired and analized using Zetasizer Malvern software. The information obtained with DLS were complemented by Zeta potential measurements, which report on the surface charge of colloidal aggregates in solution. Specifically, Zeta potential data were obtained from the electrophoretic mobility employing the Helmholtz-Smoluchowski equation[11].

SMALL ANGLE X-RAY SCATTERING (SAXS) ANALYSIS

The structural properties of plain and auxin loaded nanovectors at high resolution were determined by Small Angle X-ray Scattering (SAXS). This technique provides information about the average size and shape of particles

in solution, but also about the internal structure of the analyzed system, which can be a solution of macromolecules, nanocomposites or metal nanoparticles. The sample solution in exposed to a monochromatic beam of X-rays, whose scattering intensity, *I(q)*, is recorded at small angles of few degrees (typically 1-10°) as function of momentum transfer *q* ($q = 4\pi/\lambda \sin\theta$, where 2θ is the scattering angle between the incidence and scattered radiation).

The SAXS experiments described in this thesis were performed at the ID02 beamline of the European Synchrotron Radiation Facility (Grenoble, France). The wavelength of the incoming beam was 1 μm, and the sample detector distances was 1 m, which covered a q range 0.103-6.5 nm^{-1}. The 2D SAXS patterns initially recorded were normalized to the absolute scale using a standard procedure reported elsewhere[12,13]. Samples were loaded on a flow through capillary of 2 mm diameter to ensure accurate background (water) subtraction. Data fitting was performed by using GAP (Global Analysis Program) package[14,15], that allows to reproduce the SAXS intensity diagrams of both quasi-Bragg peaks (arising from oligolamellar structures) and diffuse scattering (originated from monolamellar vesicles).

1.2.4 APPLICATION OF NANOVECTORS TO *IN VIVO* ROOTING

One-year old olive scions were collected from plants of cultivar (cv) Leccino (easy-to-root), one of the most cultivated cultivars in Italy, and cv Leccio del Corno (difficult-to-root), an interesting cultivar for its agronomic and qualitative characteristics[9]. After the harvest, scions 3-3.5 mm in diameter were cut to a length of 10-15 cm, with 4-6 nodes and 4 leaves, to obtain semi-hardwood cuttings. Each treatment consisted of 20 cuttings per experimental

unit. After each treatment, the cuttings were transferred in greenhouse benches containing pearlite and kept under mist for 90 days. Swelling of the cutting base, callus presence, rooting percentage and number and length of roots were analyzed. Eleven treatments (T) were carried out during three independent experiments performed in January, April and July 2017 (Table 2). Cutting basal ends of Leccino and Leccio del Corno were dipped in IBA and NAA nanovectors with two different cargo concentrations, 50 ppm (T4, T5) and 200 ppm (T6, T7), and in 200 ppm cargo PE and PC formulations (T8-T11). Cuttings were soaked for 48, 72 and 96 hours in different plain pomace, PE and PC series formulations (Table 2, Experiment 1; 2; 3). Respectively two types of controls were chosen, i.e. the "standard procedure" (SP; T2, T3) usually adopted for olive propagation, and control (C; T1) in water and without hormones. For the standard procedures, powder IBA was dissolved in hydro-alcoholic solution at 4000 ppm, powder NAA was dissolved in aqueous solution at 2000 ppm and then cuttings basal ends were dipped in the solutions for 7 seconds following the recommendations of Fabbri et al.[9] For control cuttings, bases were dipped in non-loaded nanovectors and water for 48, 72 and 96 hours, respectively (Table 2).

Table 2. Rooting induction treatments in Experiment 1 (January), 2 (April) and 3 (July).

		Experiment		
Code	Treatment (T)	January (48 h)	April (72 h)	July (96 h)
T1	Control (C) *	x	x	x
T2	SP-IBA (4000 ppm)	x	x	x
T3	SP-NAA (2000 ppm)	x	x	x
T4	IBA (50 ppm)	x	-	-
T5	NAA (50 ppm)	x	-	-
T6	IBA (200 ppm)	-	x	x
T7	NAA (200 ppm)	-	x	x
T8	IPE (200 ppm)	-	x	-
T9	NPE (200 ppm)	-	x	-
T10	IPC (200 ppm)	-	-	x
T11	NPC (200 ppm)	-	-	x

* controls in water and in nanovectors without hormones, comprehensive of E, EPE and EPC (see Table 1.)

1.2.5 APPLICATION OF NANOVECTORS TO *IN VITRO* ROOTING

Canino is a widespread olive cultivar in central Italy with high and constant productivity and low susceptibility to the major diseases that affect olive[16]. Various *in vitro* studies on this cultivar have been performed[17], but no information about its rooting ability is reported. In the following experiment, four different treatments were tested on micro-cuttings (3 nodes length) of Canino (Table 3): 1) IBA 2 mg/mL loaded nanovectors, 2) non-loaded nanovectors (E), 3) IBA 2 mg/mL dissolved in aqueous solution, 4) IBA 2 mg/L added to OM (Olive medium[18]) semisolid medium (conventional method).

The liquid solutions used for rooting experiment were sterilized by filtration (Sartorius 0.45µ pore filter) and maintained under UV light for 12h. Canino micro-cuttings were soaked in 1 mL of all liquid treatments (code number 1, 2, 3 – Table 3.) under laminar flow hood in sterile conditions and covered by plastic containers to prevent dehydration (Fig. 10). The length of liquid treatment was 6 and 24 h, then the explants were placed on hormone free OM semisolid medium supplemented with 50 mg/L Fe-EDDHA, 36 g/L mannitol and 3 g/L Gelrite™. Micro-cuttings in conventional method were cultured in semisolid medium for 6 weeks. In the experiment, glass jars (500 mL) with 100 mL of semisolid OM medium containing 6 micro-cuttings each were employed, for a total of 12 jars and 72 micro-cuttings. All jars were maintained at 22°C±1°C, under a 16h light/ 8h dark photoperiod at 60 µmol m^{-2} s^{-1} photosynthetically active radiation provided by cool-white fluorescent lamps. To favor root emission, the basal area of the micro-cuttings was kept in the dark by covering the base of the jars. Rooting percentage of micro-cuttings was evaluated after 6 weeks.

Table 3. Treatments on micro-cuttings cv Canino.

		Lenght liquid treatment	
Code	Treatments	(h)	(h)
1	IBA (nanovectors)	6	24
2	E (empty nanovectors)	6	24
3	IBA liquid	6	24
4	IBA 2mg/L medium	-	-

1.2.6 STATISTICAL ANALYSIS

Data from *in vivo* tests were not normally distributed (Kolmogorov-Smirnov one-sample test) and were therefore analyzed using the non-parametric Kruskal-Wallis rank-sum test followed by the Mann-Whitney U Test for multiple comparisons between different treatments. Differences were accepted when significant at the 5% level. Statistical analyses were performed using SYSTAT 12.0 software (Systat Software Inc., San Jose, CA, USA).

1.3 RESULTS AND DISCUSSION

1.3.1 CHARACTERIZATION OF THE NANOVECTORS

DYNAMIC LIGHT SCATTERING AND ZETA POTENTIAL

DLS data showed that aggregates with mean size in the range 170-400 nm were formed both by the natural lipid (pomace series: E, IBA and NAA) and composite formulations with DOPE (PE series: EPE, IPE and NPE) or DOPC (PC series: EPC, IPC and NPC), as shown in Figure 4. The polydispersity index (PdI) of all samples was in the range 0.2-0.4, indicating the presence of scattering objects with wide but controlled size distribution. The observed polydispersity was consistent with the structural complexity expected for these systems. Nevertheless, all samples were stable over time, as checked by repeated DLS measurements. All suspensions remained monophasic and homogeneous even after 4-6 months. The main differences were observed as a function of lipid composition. In particular, samples of the PE series (Fig. 4B) had smaller average dimensions (200-230 nm), with respect to samples from pomace only or to the PC series (350-400 nm, Fig.4A and 4C), thus evidencing the ability of DOPE to impart size control and improve monodispersity (Fig. 5). All nanovectors prepared with purified phospholipids showed narrower size distribution with respect to pomace lipids (Fig. 4). Moreover, aggregates containing purified lipids (either of the PE or PC series) did not show any marked size change due to the cargo loading, whereas for samples of the series prepared from pomace lipids only, the average dimensions increased upon association with auxins. This confirmed that in the absence of purified phospholipids the size and distribution of nanoaggregates were less

controlled and, consequently, guest molecules were able to easily induce variations.

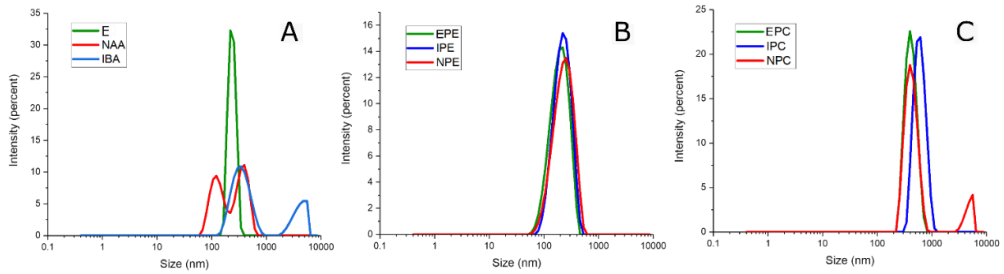

Figure 4. Size distributions obtained from Dynamic Light Scattering intensity, showing comparison among samples with different lipid composition. In each graph samples curves from the same series are reported, i.e. pomace only (4A), PE (4B) and PC (4C), pointing out differences in size and monodispersity based on the lipids employed in each one.

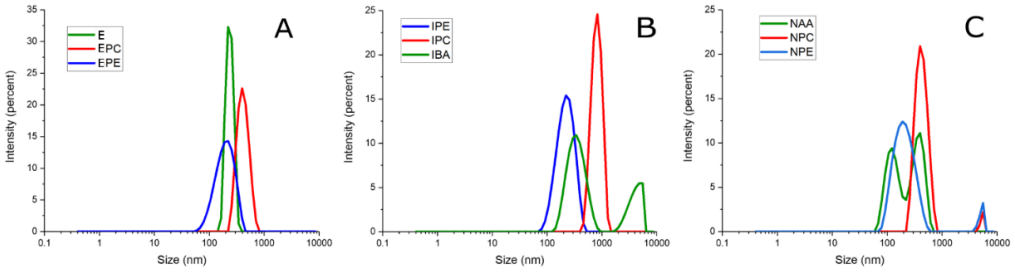

Figure 5. Dynamic Light Scattering intensity distributions as a function showing comparison among the plots made by taking into account the loaded compound. In the same graph samples from the three series loaded with the same molecule are plotted, i.e. no compound (5A), IBA (5B) and NAA (5C), to assess the presence (or absence) of trends in size and monodispersity depending on the cargo.

Concerning the surface charge, all samples had negative Zeta potential (≈-23÷ ≈-13 mV) and conductivity were in the range 0.03-0.08 mS/cm (Table 4). After auxin loading, all nanovectors showed slightly less negative surface charge with respect to the corresponding empty systems, in line with the neutrality of the inserted molecules, expected to dilute the overall surface charge.

Only pomace series	ZP (mV)	PE series	ZP (mV)	PC series	ZP (mV)
E	-19.4	EPE	-22.4	EPC	-17.6
IBA	-16.3	IPE	-23.5	IPC	-13.4
NAA	-16.5	NPE	-23	NPC	-13.6

Table 4. Zeta potential (ZP) values for the three series of samples. Error value calculated over three different runs was ± 0.2 mV.

SMALL ANGLE X-RAY SCATTERING

The scattering intensity of the formulations made from only pomace showed unstructured SAXS profiles, indicating that very polydisperse aggregates (i.e. liposomes) were in solution (Fig. 6, green curve). The presence of DOPE or DOPC, even though added in small percentage, significantly modified the SAXS curves (Fig. 6, red and blue curve). In the case of samples from PC series (blue curve), SAXS diagrams were dominated by the large oscillations pattern characteristic of monolamellar vesicles. However, the presence of a quasi-Bragg correlation peak (Fig. 6A) indicated that a fraction of bilamellar aggregates was present[19]. The other systems with the same lipid composition (EPC, IPC) showed similar patterns, suggesting a prevalence of monolamellar liposomes in solution.

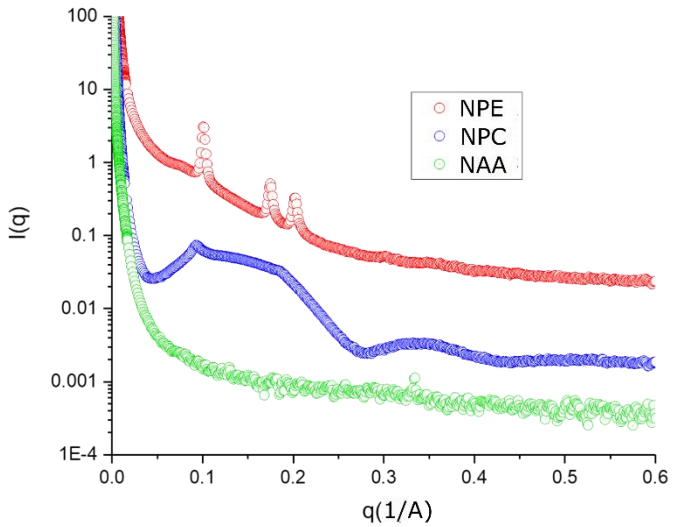

Figure 6. SAXS Intensity diagrams (I(q) vs q, curves shifted vertically for clarity) of samples loaded with NAA for each series, showing the different patterns due to the employed lipid.

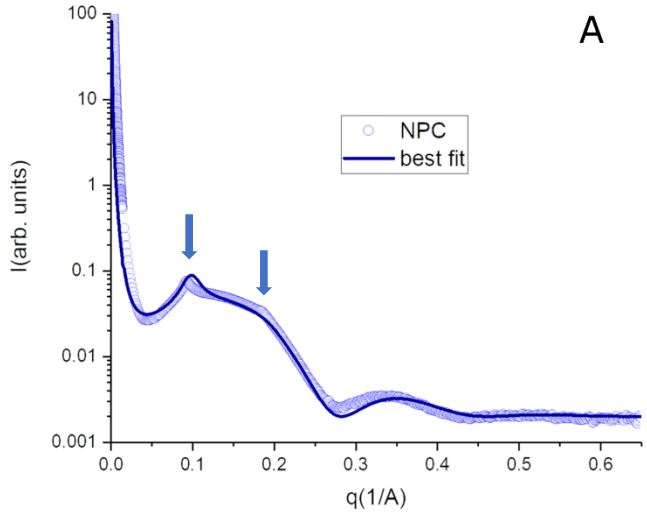

Figure 6A. SAXS diagram and best fit for sample loaded with NAA of the PC series (arrows on the peak indicating the presence of bilamellar aggregates).

For samples of the PE series, the observed SAXS profile was characteristic of a more ordered structure, i.e. a lyotropic phase, as evidenced by three well defined Bragg peaks (Fig. 7) with maxima in the ratio 1: √3: 2, typical of a hexagonal arrangement. This was consistent with the higher local curvature that DOPE is able to impart[20].

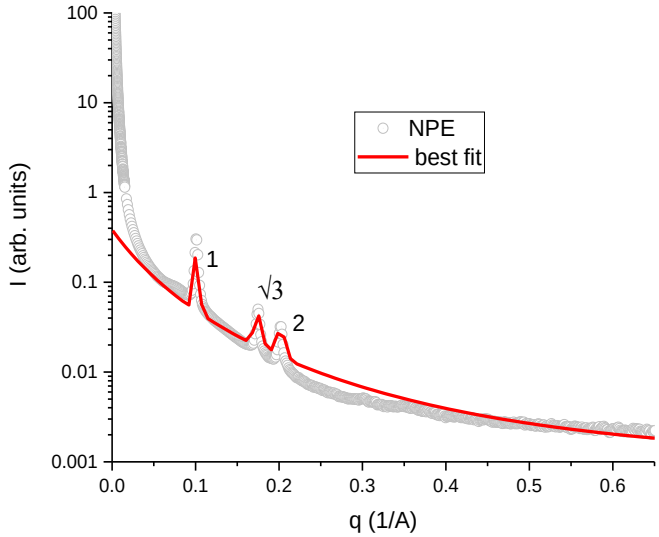

Figure 7. SAXS diagram and corresponding best fit for the sample loaded with NAA of the PE series, showing the ratios of the relative positions of the Bragg peaks.

Mass spectrometry analysis were also performed to assess the loading ability of the nanovectors. Data were provided by the CISM center of Sesto Fiorentino (Florence), and a loading capacity ranging from 200 to 300 ppm was measured. The loading efficiency, expressed as percentage of the lower starting concentration (i.e. 500 ppm), was attested around 60%, corresponding to about a 1:4 auxin/lipid molar ratio.

1.3.2 APPLICATION OF NANOVECTORS TO *IN VIVO* ROOTING

The efficacy of the auxin-delivering nanovectors was tested on olive tree cuttings of the two different cultivars easy-to-root "Leccino" and difficult-to-root "Leccio del Corno". In the first experiment conducted in January 2017, after 90 days from exposure to IBA and NAA loaded nanovectors at 50 ppm concentration for 48 h, for all treatments cv Leccino showed 65% of cuttings with swollen base and callus, while cv Leccio del Corno exhibited only callus in 25% of cuttings. Callus formation can be important in the rooting of olive cuttings since in several cultivars a close correlation was observed between callus development and rooting[9]. In any case, rooting process was observed only in cv Leccino, with a percentage of rooted cuttings in T4 (IBA 50 ppm) of 15% with an average root length of 0.4 cm, (Fig. 8A). In T2 (SP-IBA) 10% of rooting with 0.8 cm of roots length was observed. No rooting was observed in all control treatments (Fig. 8A). Exposing the cuttings to only pomace (T6, T7) and IPE and NPE (T8, T9) nanovectors loaded with IBA and NAA at 200 ppm for 72 h (Experiment 2, April 2017), the cvs Leccino and Leccio del Corno presented swollen base and callus in 24% and 10% of the cases, respectively. Rooting process was present only in Leccino and the maximum rooting percentage was observed in T6 and T8 treatment (Fig. 8B) with, respectively,

7 and 25 mean number of fully developed roots, and an average length of 1.8 and 2.2 cm in both treatments (Fig. 9B and 9C). Interestingly, rooting was observed also in NPE (NAA-DOPE) nanovectors (T9), with 10% of rooting, an average of 18 roots, which length ranged from 1.5 to 1.7 cm (Fig. 9D), while the cuttings dipped in NAA standard (T3) or in NAA nanovectors (T7) did not show roots.

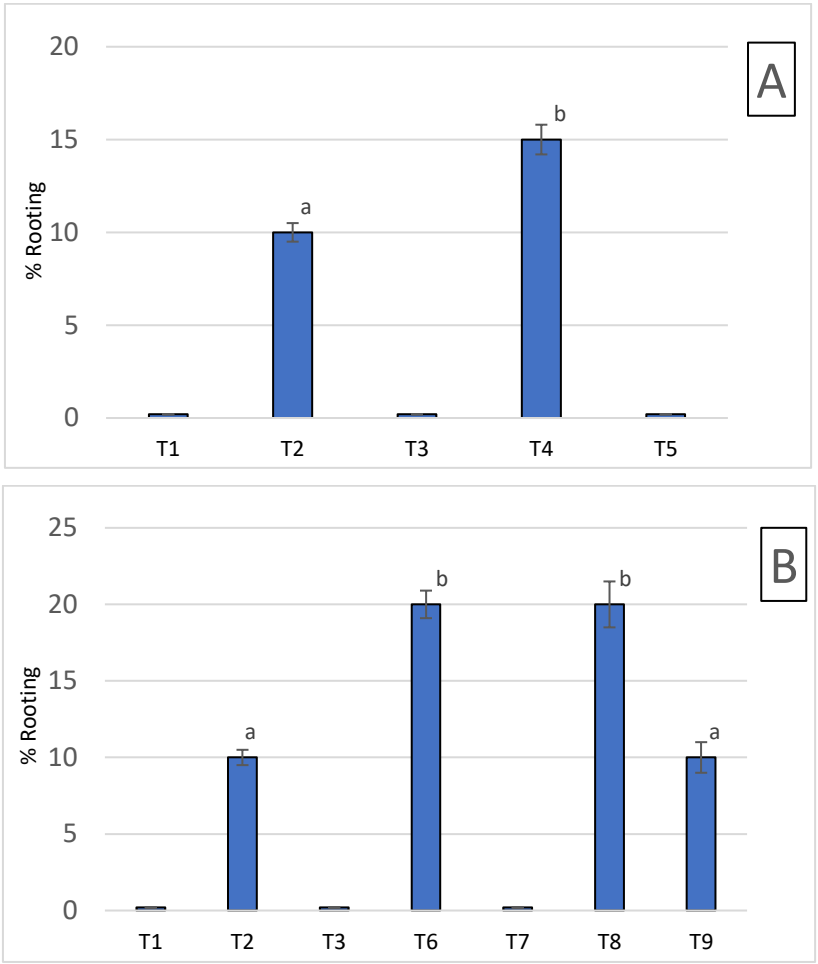

Figure 8. Rooting percentage of Leccino cv cuttings in January (Experiment 1: graph A) and in April (Experiment 2: graph B). Error bars represent standard error values. Graph A: different letters indicate a significant difference by Mann-Withney U test (p-value < 0.05; d.f.=1). Graph B: different letters indicate a significant difference by

Kruskal-Wallis test ($\chi^2 = 13.40$; p-value < 0.001; d.f.=3) followed by Mann-Withney U test for multiple comparisons.

In T2 treatment, the percentage of rooted cuttings was of 10%, while no rooting was observed in all control treatments.

In a third experiment (July 2017), after 90 days a high percentage of Leccino and Leccio del Corno cuttings (more than 95%), soaked in nanovectors (T6, T7, T10, T11 treatments), showed signs of basal rot (Fig. 9E, red arrow) though many examples of callous formation were observed (Fig. 9E and 9F, green arrows).

Figure 9. Experiment 1 - Rooting effect of *in vivo* cultured cv Leccino cuttings treated

with IBA loaded nanovectors 50 ppm (A): callus formation, roots emission and swelling of the base; Experiment 2 - Fully developed root in *in vivo* cultured cv Leccino cuttings treated with IBA 200 ppm loaded nanovectors (B), IPE loaded nanovectors (C) and NPE loaded nanovectors (D); Experiment 3 – Callus formation in *in vivo* cultured cv Leccino cuttings treated with NPC loaded nanovectors (E) and IPC loaded nanovectors (F): basal rot (red arrows), callus formation (green arrows) and root emission (black arrow).

Nevertheless, in T10 treatment one cutting had root emission (Fig. 9F black arrow). In T2 and T3 standard treatments, cuttings showed neither basal rot nor rooting, as expected for the brief soaking time of this procedure. The cuttings of all controls (T1) showed no sign of root formation.

In olive trees, the success of rooting process can be affected by many factors, included the type of cultivar and the timing of cutting collection[9]. The results of a screening on rooting rate of 426 cultivars reported that more than 60% of cultivars present a low rooting ability (0-33%), 20% have a medium rooting ability (33-66%) and only 16% of the total show a rate of rooting higher than 70%. The most suitable season for cutting preparation coincides with the two annual peak points of April–June (summer cycle), when vegetative growth is at its peak, and of September-October (autumn cycle), before the physiological activity of the plant decreases due to the low winter temperatures[9]. *In vivo* results confirmed the higher rooting ability of cv Leccino compared to cv Leccio del Corno. Furthermore, this study reported that cv Leccino cuttings, dipped in IBA nanovectors in January, emitted roots, thus suggesting that the application of loaded nanovectors could increase the period of propagation of the cultivars in the nursery. In the second experiment, carried out in a favorable period for rooting, the aforementioned

results were confirmed, and the addition of PE nanocarriers in treatments with both hormones favored the rhizogenic effect and increased the roots number and length. This is in line with the enhanced control imparted by DOPE on nanovectors design, stability and cargo release, even in the case of NAA, the less bioavailable auxin. Moreover, the data revealed that 96h dipping, regardless of the treatment applied, is unsuitable for olive rooting. However, even in these unfavorable conditions, PC nanovectors induced swollen basal end (Fig. 9E), which could prelude to subsequent root emission (Fig. 9F). In this case further protocol adjustments need to be explored.

In this research, the treatment with hormones encapsulated in nanocarriers enhanced rooting process, this effect might be due to improved hormone bioavability and easier accumulation, with supposedly a slow release in the basal part of the cutting.

1.3.3 APPLICATION OF NANOVECTORS TO *IN VITRO* ROOTING

The efficacy of the auxin-loaded nanovectors was then assessed in Canino cv; these micro-cuttings were soaked in liquid treatment for 6 hours and then transferred into OM semisolid medium for 6 weeks (Fig. 10). Results showed a higher percentage of root development in micro-cuttings exposed to IBA loaded nanovectors (27%) than the one registered for micro-cuttings treated with liquid IBA (18%) (Fig. 11). The extension of the length of treatment to 24h was not effective in increasing the percentage of rooting, being it reduced to 16% in the case of IBA loaded nanovectors and to10% in liquid IBA (Fig. 11). Moreover, a prolonged treatment revealed symptoms of suffering in micro-cuttings. The treatment with non-loaded formulations (E), both at 6 and 24h, showed some callus formation and no rooting in micro-cuttings (Fig. 12A).

Semisolid medium with conventional IBA administration recorded 16% of rooting (Fig. 12B), similar to IBA liquid after 6h, but poor rooting was produced in this treatment with respect to 6h IBA loaded nanovectors application (Fig. 12 C, D, E). *In vitro* cultures treated with nanovectors showed less contamination compared to non-loaded nanovectors ones.

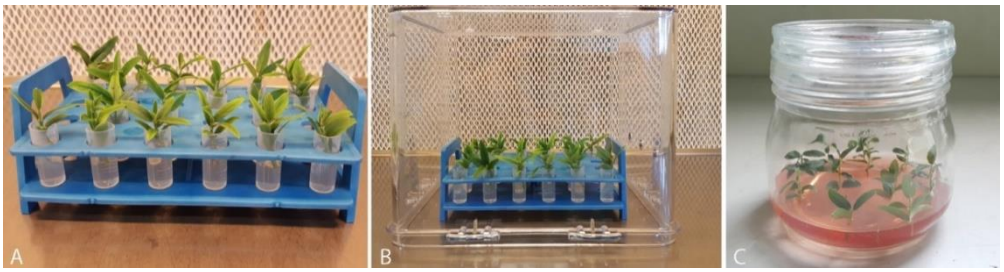

Figure 10. *In vitro* olive micro-cuttings: A, B during treatment with nanovectors loaded with IBA for 6h; C micro-cuttings transferred in OM semisolid medium for 6 weeks.

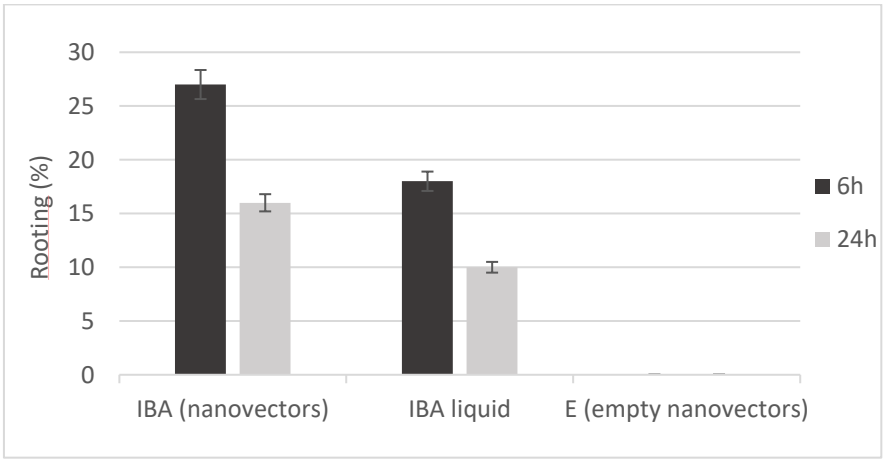

Figure 11. Rooting percentage after 6 and 24h liquid pulse treatments in Canino micro-cuttings. Error bars represent standard error values.

Figure 12. *In vitro* olive micro-cuttings rooting after 6 weeks. A: callus formation after treatment with non-loaded nanovectors; B: roots development in treatment with IBA added in OM semisolid medium and C, D, E after treatment of 6h with IBA loaded nanovectors.

Therefore, 6h liquid pulse treatment with loaded nanovectors at the concentration of 2 mg/mL was associated with more favorable emission and development of roots. The rooting micro-cuttings were in healthy conditions, thus further confirming the compatible and non-toxic nature of these treatments. The same condition was recorded also in micro-cuttings without roots treated with empty nanovectors. Phytotoxic effect is an aspect that needs to be taken into account and the lipid-based nanovectors used in this study, being of plant origin because deriving from olive pomace, did not show any visual sign of toxicity on the micro-cuttings.

In *in vitro* culture, in most cases, the culture medium is directly supplemented with IBA, before autoclaving, at the rate increasing from 1 to 4 mg/L to obtain highest rooted explants and root quality. In this research, the application of 2 mg IBA in conventional method showed lower rooting percentage in respect to other *in vitro* olive cultivars. However, rooting ability vary significantly among different olive cultivars[9]. Regarding the sterilization method of liquid solutions, filtration and UV irradiation procedures have been considered, as the elevated temperatures used for autoclaving are not suited for the stability of lipid-based nanovectors.

1.4 CONCLUSIONS

In this project, olive pomace was employed as lipid source for the development of nanocarriers delivering auxins as root-promoting phytohormones, and a new methodology for phytohormones' administration was experimented on olive cuttings obtained from three different cultivars (cv Leccino, cv Leccio del Corno and cv Canino). In two of these, the nanovectors-mediated treatment of the cuttings was found to improve the rooting process with respect to the conventional treatments, both *in vivo* (Leccino cv) and *in vitro* (Canino cv). These preliminary results represent a significant initial step for further investigations of the nanovectors' potentialities of application to olive trees.

1.5 REFERENCES

[1] Hossain, L., Rahman, R., & Khan, M. S. (2017). Alternatives of pesticides. In Pesticide residue in foods (pp. 147-165). Springer, Cham.

[2] Khot, L. R., Sankaran, S., Maja, J. M., Ehsani, R., & Schuster, E. W. (2012). Applications of nanomaterials in agricultural production and crop protection: a review. *Crop protection*, *35*, 64-70.

[3] Ranjan, S., Dasgupta, N., & Lichtfouse, E. (Eds.). (2016). *Nanoscience in Food and Agriculture*. Cham: Springer International Publishing.

[4] Angelova, A., Garamus, V. M., Angelov, B., Tian, Z., Li, Y., & Zou, A. (2017). Advances in structural design of lipid-based nanoparticle carriers for delivery of macromolecular drugs, phytochemicals and anti-tumor agents. *Advances in colloid and interface science*, *249*, 331-345.

[5] Roy, I., Ohulchanskyy, T. Y., Pudavar, H. E., Bergey, E. J., Oseroff, A. R., Morgan, J., ... & Prasad, P. N. (2003). Ceramic-based nanoparticles entrapping water-insoluble photosensitizing anticancer drugs: A novel drug− carrier system for photodynamic therapy. *Journal of the American Chemical Society*, *125*(26), 7860-7865.

[6] Li, N., Zhuang, C., Wang, M., Sun, X., Nie, S., & Pan, W. (2009). Liposome coated with low molecular weight chitosan and its potential use in ocular drug delivery. *International journal of pharmaceutics*, *379*(1), 131-138.

[7] Gómez-Muñoz, B., Hatch, D. J., Bol, R., & García-Ruiz, R. (2012). The compost of olive mill pomace: from a waste to a resource-environmental benefits of its application in olive oil groves. *Sustainable Development-Authoritative and Leading Edge Content for Environmental Management*, 459-484.

[8] Saini, S., Sharma, I., Kaur, N., & Pati, P. K. (2013). Auxin: a master regulator in plant root development. *Plant cell reports*, *32*(6), 741-757.

[9] Fabbri, A., Bartolini, G., Lambardi, M., & Kailis, S. (2004). *Olive propagation manual*. Landlinks Press.

[10] Koppel, D. E. (1972). Analysis of macromolecular polydispersity in intensity correlation spectroscopy: the method of cumulants. *The Journal of Chemical Physics*, *57*(11), 4814-4820.

[11] Hunter, R.J. (1981). Zeta Potential in Colloid Science. London, England: Academic Press

[12] Zemb, T., & Lindner, P. (Eds.). (2002). *Neutrons, X-rays and light: scattering methods applied to soft condensed matter*. North-Holland.

[13] Boesecke, P. (2007). Reduction of two-dimensional small-and wide-angle X-ray scattering data. *Journal of Applied Crystallography*, *40*(s1), s423-s427.

[14] Pabst, G., Rappolt, M., Amenitsch, H., & Laggner, P. (2000). Structural information from multilamellar liposomes at full hydration: full q-range fitting with high quality x-ray data. *Physical Review E*, *62*(3), 4000.

[15] Pabst, G., Koschuch, R., Pozo-Navas, B., Rappolt, M., Lohner, K., & Laggner, P. (2003). Structural analysis of weakly ordered membrane stacks. *Journal of Applied Crystallography*, *36*(6), 1378-1388.

[16] Bartolini G. 2008, Oleadatabases http://www.oleadb.it/

[17] Rugini, E., Cristofori, V., & Silvestri, C. (2016). Genetic improvement of olive (Olea europaea L.) by conventional and *in vitro* biotechnology methods. *Biotechnology advances*, *34*(5), 687-696.

[18] Rugini, E. (1984). *In vitro* propagation of some olive (Olea europaea sativa L.) cultivars with different root-ability, and medium development using

analytical data from developing shoots and embryos. *Scientia Horticulturae*, *24*(2), 123-134.

[19] Kucerka, N., Pencer, J., Sachs, J. N., Nagle, J. F., & Katsaras, J. (2007). Curvature effect on the structure of phospholipid bilayers. *Langmuir*, *23*(3), 1292-1299.

[20] Siegel, D. P., & Epand, R. M. (1997). The mechanism of lamellar-to-inverted hexagonal phase transitions in phosphatidylethanolamine: implications for membrane fusion mechanisms. *Biophysical journal*, *73*(6), 3089-3111.

SECTION 2. *NANNOCHLOROPSIS*-DERIVED NANOVECTORS FOR THE DELIVERY OF THYMOL

2.1 INTRODUCTION

The employment of traditional pesticides is currently representing a worldwide problem that can no longer be postponed due to the serious impact that these agrochemicals display on the environment and, consequently, on human health too.

In the last years, the increasing demand for natural products as substitutes, or to integrate the conventional ones, has received a great attention from the scientific community, which is attempting to find a sustainable and more environmentally friendly way to control plant diseases and pests[1]. Possible alternatives include the use of plant-derived antimicrobial compounds, like terpenes and terpenoids, which are the main constituents of the essential oils extracted from a large variety of plants and flowers[2,3]. Peculiar pharmacological properties, such as antibacterial, antifungal, anti-inflammatory and antioxidant activity[4], make this class of compounds an attractive resource for many different applications in the field of medicine, agrotechnology, food industry and cosmetics, to mention only a few. This complex and very large class of secondary metabolites plays an important role in plant defense against herbivores and pathogens attack, encouraging researchers towards a deeper understanding of the underlying mechanisms of actions of these molecules[5].

On the other hand, the volatile nature of terpenes and terpenoids represent one of the major drawbacks in terms of long-term efficacy, that certainly must be addressed in the developing of new commercial phytochemicals.

Moreover, the hydrophobic character of many of these compounds, some of which are insoluble in water, requires the design of an *ad hoc* formulation able to ensure the effectiveness of the product. In this context, lipid nanovectors, such as liposomes and solid lipid nanoparticles, represent an interesting nanotechnological platform to be further investigated. Their lipid structure displays multiple benefits: the membrane-like structure promotes biocompatibility and a non-toxic interaction with the target cell. At the same time, it acts as a protective shell that prevents degradation processes and volatilization of guest molecules[6]. Concerning the interaction between lipid structures and terpenes/terpenoids, these lipophilic compounds exhibit a marked preference for hydrophobic phases, which act as sites of accumulation[2]. Hence, the loading into the carriers is highly favored. Thanks to the aforementioned characteristics, lipid nanovectors fully meet the requirements needed for a successful association with these natural antimicrobial agents.

Several studies report the higher antimicrobial activity of oxygenated and phenolic terpenoids in respect to hydrocarbon terpenes[2,7]. The presence of a hydroxyl group and a system of delocalized electrons in their structure is indeed thought to be crucial and strictly related to their higher efficacy as antibacterial agents. Thymol is an oxygenated phenolic monoterpenoid which was found to be the most effective antimicrobial among the constituents of essential oils[8]. It can be extracted from many aromatic plants, *Thymus vulgaris* being the principal one, and its indirect employment is historically documented since the time of ancient Egyptians and Greeks, who used thyme as food-preservative and flavoring agent[9]. Therefore, thymol was selected as vectors' drug, among a wide variety of isoprenoid compounds.

In this work, the possibility of a thymol-delivery via lipid vectors was investigated and a green design was adopted for the realization of the nanoparticles. The lipids employed in the manufacturing were extracted from the marine microalga *Nannochloropsis* sp., an autotrophic microorganism chosen for its high natural lipid content, ranging from 39 to 68% of the total biomass[10]. There is a twofold advantage in the use of this microalga for the vectors' fabrication: its easiness of cultivation allows to obtain large amounts of biomass, and the high lipid content leads to a good yield of extraction, thus reducing the wastes of raw material.

The aim of this work was the production of lipid nanovectors employing lipids extracted from a photosynthetic biosource, to develop an eco-sustainable agrotechnological tool improving thymol long-term efficacy as antibacterial agent. A small amount of dioleoylphosphatidylethanolamine (DOPE), a purified neutral phospholipid, was also added to the lipid extract as a helper co-lipid, in order to facilitate nanovectors' structuring.

The characterization of the lipid fraction extracted from *Nannochloropsis sp.* and the determination of the thymol loaded into the obtained nanovectors were both performed via GC-MS analysis. Dynamic light scattering measurements provided key information about the dimension and distribution of the particles in solution and were complemented by zeta potential measures. A detailed structural characterization of the aggregates was obtained by small-angle X-ray scattering and finally, their efficacy as antibacterial formulation was tested *in vitro* against the plant pathogen *Xanthomonas campestris* pv. *vesicatoria* (Xcv).

This bacterium is the causal agent of bacterial leaf spot (BLS) in tomato (*Lycopersicon esclulentum* Mill.) and pepper (*Capsicum annuum* L.) plants,

causing serious damages to fruit quality and production[11]. The conventional way to control plant bacterial diseases is the repeated application of copper compounds, which help to prevent bacterial infections, but has been shown to be harmful to the environment. In fact, copper is a heavy metal and accumulates in soil and water[12]. In addition, many bacterial strains of the genus *Xanthomonas* were found to develop resistance to copper treatments, giving proof of the serious consequences implied in copper compounds routinely applications[13]. Therefore, alternative solutions must be found, and essential oils and their constituents are definitely very promising candidates, as evidenced by numerous scientific publications[2,3,10]. For instance, a study by Dadasoglu et al. (2011) evidenced the effectiveness of thymol and the essential oils extracted from three *Origanum* species against a phytopathogenic *Xanthomonas* species responsible for BLS disease[3].

In this project, an eco-compatible and biodegradable nanosystem tailored to obtain the delivery of a volatile and lipophilic drug was developed, and Xcv was chosen as target microorganism.

2.2 MATERIALS AND METHODS

2.2.1 REAGENTS

1,2-Dioleoyl-sn-glycero-3-phosphoethanolamine (DOPE) and soybean phosphatidylcholine (S100) were purchased from Lipoid GmbH (Ludwigshafen am Rhein, Germany). Agar and Nutrient Broth were purchased from Sigma-Aldrich and D-glucose was from Carlo Erba.

2.2.2 EXTRACTION OF THE LIPID FRACTION FROM *NANNOCHLOROPSIS* SP.

Dry and powdered biomass of *Nannochloropsis* sp. (2g) was provided by the microalgae cultivation-specialized laboratory of the Department of Agriculture, Food, Environment and Forestry (DAGRI), University of Florence. The microalga was grown in nitrogen-deprived condition and the lipid content was expected to reach up to 68% of the total biomass.

Lipid extraction procedure:

- Weigh 15 mg of dry biomass per each screw-capped glass tube (tube 1)
- Add 250 µl $CHCl_3$: MeOH (1:2, v/v) and glass beads, then vortex for five minutes
- Add 750 µl $CHCl_3$: MeOH (1:2, v/v) and heat at 60 °C for three minutes
- Collect the supernatant in a second glass tube (tube 2) and rinse the glass beads as follows:
    - Three times with 0.5 $CHCl_3$: MeOH (1:2, v/v)
    - Twice with 1 mL $CHCl_3$: MeOH (1:2, v/v)
- Centrifuge at 5000 rpm for five minutes and collect the supernatant in a glass tube (tube 3)
- Add 1.5 mL $CHCl_3$: MeOH (1:2, v/v)
- Add 1.5 mL MilliQ water
- Vortex the glass tube and centrifugate at 5000 rpm for five minutes
- Collect the lower chloroform phase in a glass tube (tube 4)
- Rinse tube 3 with 1 mL $CHCl_3$, vortex, centrifuge as previously described and transfer the lower phase in tube 4
- Evaporate the solvent and weight the dry lipid fraction extracted

The yield of lipid extraction was calculated as follows:

$YE = (DB_2/DB_1) \times 100\%$

where YE (w/w) was the Yield of Extraction (%), DB_2 was the dry weight of the biomass after the extraction and DB_1 was the dry weight of the biomass pre-extraction.

2.2.3 FABRICATION OF NANOVECTORS

Nannochloropsis-derived nanovectors (N-NVs)

Thymol ($C_{10}H_{14}O$) and 1,2-dioleoyl-sn-glycero-3-phosphoethanolamine ($C_{41}H_{78}NO_8P$) (15% w/w) as adjuvant lipid were added to the lipid fraction obtained from the extraction procedure above described. Both were dissolved in chloroform and the proper amount of thymol stock solution was added to get a lipid/thymol 5:1 molar ratio. Finally, the solvent was evaporated, and a thin film was formed. Rehydration with MilliQ water and nine freezing and thawing cycles (i.e. soaking in liquid nitrogen, vortexing and then dipping samples in a warm bath at 45 °C) promoted lipid molecules' self-assembly into particles whose dimensions were homogenized by four sonication cycles of four minutes each (at 95% power, with a probe equipped Sonopuls Bandelin ultrasonic homogenizer). Samples were sterilized by exposure to U.V. light under laminar flow hood for five hours of treatment, covered by parafilm to prevent dehydration and then stored in a refrigerator at 4°C.

Soybean phosphatidylcholine nanovectors (S100-NVs)

A set of nanovectors made of soybean phosphatidylcholine (S100) was also prepared to compare a purified lipid nanoformulation with the *Nannochloropsis*-derived one. The same preparation procedure was followed with the exception of the extraction step, as purchased purified lipids (Lipoid S 100) were employed.

A summary table of the NVs' composition is reported (Table 5), whilst molecular structures of employed compounds are shown in figure 13.

N-NVs	Sample acronym	Lipid from N. sp (mg)	DOPE (mg)	Thymol (mg)	Volume of sample (mL)	Lipid concentration (mg/mL)
Thymol-loaded	N T	570	100.58	28.78	22.35	30
Plain	N B	160	28.26	0	6.27	30

*N=*Nannochloropsis* sp.; N-NVs=*Nannochloropsis*-derived nanovectors.

Purified lipid NVs	Sample acronym	Phosphatidylcholine (mg)	Thymol (mg)	Volume of sample (mL)	Lipid concentration (mg/mL)
Thymol-loaded	S100 T	270	11.6	9	30
Plain	S100 B	180	0	6	30

Table 5. Detailed composition of *Nannochloropsis*-derived NVs (N-NVs) and purified lipid-NVs (S100-NVs). The lipid concentration, together with the final volume of the samples, are also reported.

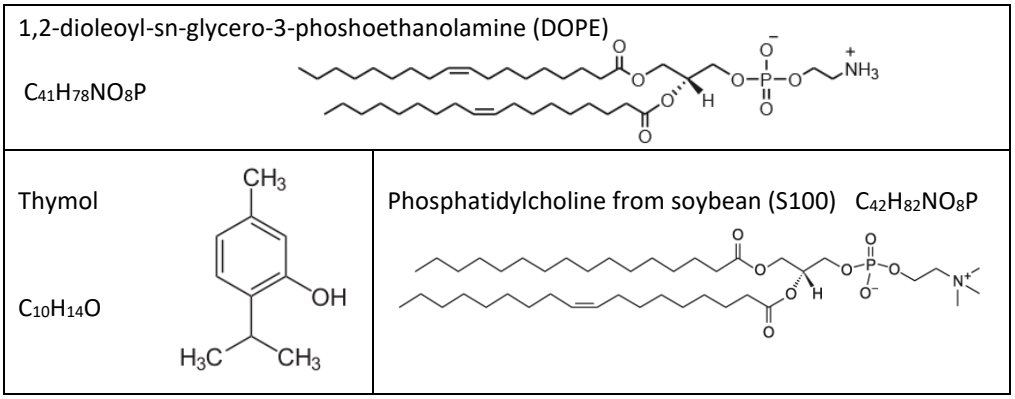

Figure 13. Molecule structures of thymol and phospholipids employed in nanovectors' fabrication.

2.2.4 NANOVECTORS' STRUCTURAL CHARACTERIZATION

DYNAMIC LIGHT SCATTERING AND ZETA POTENTIAL MEASUREMENTS

See description at paragraph 1.2.3

SMALL ANGLE X-RAY SCATTERING (SAXS) ANALYSIS

See description at paragraph 1.2.3

2.2.5 GC-MS ANALYSIS: QUANTIFICATION OF THYMOL LOADED INTO NANOVECTORS AND DETERMINATION OF THE FATTY ACID COMPOSITION OF *NANNOCHLOROPSIS* SP.

QUANTIFICATION OF THYMOL

Extraction

The thymol content was determined by gas chromatography-mass spectrometry technique.

The extraction of thymol was performed as follows: 80 µL of nanovectors in aqueous solution were mixed with an equal volume of methanol and heptane. Methanol was added to break the lipid aggregates and heptane containing

tridecane 20 ppm as internal standard, was used as extraction solvent. Samples were then vortex-mixed for five minutes, sonicated for fifteen minutes and kept on over-night rotary agitation. After centrifugation at 4000 rpm for ten minutes, the heptane phase was collected for the GC-MS analysis.

Determination of Thymol partition coefficient

As lipid nanovectors are aqueous samples and thymol is partially soluble in water (0.98mg/mL), its heptane/water partition coefficient was determined using a stock solution of thymol in heptane 25 ppm concentrated. The final concentration of the samples was adjusted according to this coefficient.

A scheme of the extraction setting adopted to determine thymol partition coefficient and thymol content is reported in figure 14.

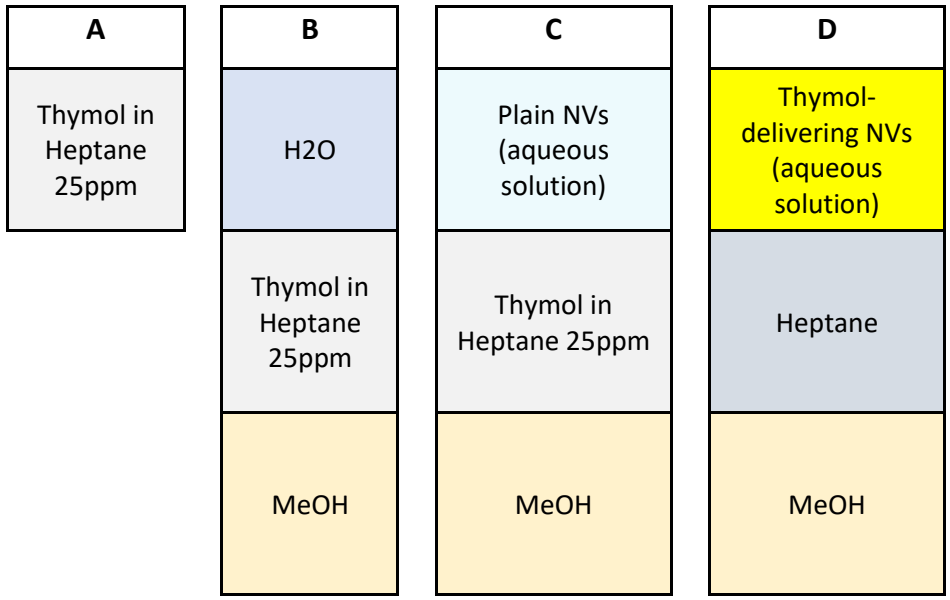

Figure 14. In a glass GC-MS vial were respectively added: **A**) 80 µL of 25 ppm thymol in heptane stock solution; **B**) 80 µL of 25 ppm thymol in heptane stock solution, 80 µL of MilliQ water, 80 µL of methanol MeOH; **C**) 80 µL of 25 ppm thymol in heptane

stock solution, 80 µL of plain nanovectors (NVs) in water solution, 80 µL of MeOH; **D**) 80 µL of heptane-tridecane, 80 µL of thymol-delivering NVs in water solution, 80 µL of MeOH.

GC-MS analysis

An Agilent 7820 Gas Chromatograph system equipped with a 5975C MSD with EI ionization was employed, all from Agilent Tech. (Palo Alto, AC, USA). One µL of extract in solvent was injected in a split/splitless injector operating in splitless. A Gerstel MPS2 XL autosampler equipped with liquid option was used. The chromatographic settings were as follows: injector in splitless mode set at 260 °C, J&W innovax column (30 m, 0.25 mm i.d., 0.5 µm df); oven temperature program: initial temperature 40 °C for 1 min, then 5 °C min^{-1} until 200 °C, then 10 °C min^{-1} until 220 °C, then 30 °C min^{-1} until 260 °C, hold time 3 min. The mass spectrometer was operating with an electron ionisation of 70 eV, in scan mode in the m/z range 29-330, at three scans sec^{-1}.

In order to quantify the analyte, thymol calibration curve was constructed by injecting known concentrations of thymol (1.25 ppm, 2.5 ppm, 5 ppm, 10 ppm, 20 ppm, 40 ppm, 80 ppm, 160 ppm) into the gas chromatograph-mass spectrometer. Data was acquired and analyzed using Agilent MassHunter software.

FATTY ACID COMPOSITION OF *NANNOCHLOROPSIS* SP.

The lipid fraction was extracted following the procedure described at 2.2.2, then the three different lipid classes were separated through chromatographic fractionation in order of polarity: neutral lipids

(hydrocarbons, free fatty acid and sterols), glycolipids and polar lipids (phospholipids).

Lipid fractionation

The lipid fractionation was performed as follows: the dry lipid extract was weighted, resuspended in chloroform and vortexed. 100 µL were introduced in a chromatography column (Bond Elut SI, Agilent) and the three different fractions containing neutral lipid, glycolipids and phospholipids were collected in screw-capped glass vials washing the column respectively with 1 mL of chloroform, 1 mL of acetone and 1 mL of methanol. Samples were heated at 60 °C and taken to dryness under liquid nitrogen.

Derivatization of the fatty acids

The esterified fatty acids obtained for each lipid class were transformed in the corresponding methyl esters via alkaline transmethylation reaction. 500 µL of methanol:toluene (1:1, v/v), 100 µL of KOH in MeOH 2 M and 10 µL of nonadecanoic acid (230 ng/µL) as internal standard, were added to the extracts. Samples were heated at 60 °C in a thermoblock heater for 15 minutes to allow transesterification reaction to occur. 1 mL of hexane:chloroform (4:1, v/v), 300 µL of acetic acid 1 M and 1 mL of MilliQ water were added and samples were vortex-mixed for one minute. After centrifugation at 3000 rpm for five minutes, the upper organic phase was collected, and methyl esters were analyzed through GC-MS. A Fatty Acids Methyl Esters (FAMEs) standard mix, also added with nonadecanoic acid as internal standard, was employed to generate a four levels calibration curve. GC-MS analysis was performed as previously described and analytes were

identified comparing their Retention Time (RT) with those of the standard mix and matching the mass spectra acquired with those obtained from the standards and/or published in the NIST Mass Spectral Database.

2.2.6 NANOVECTORS' ANTIBACTERIAL ACTIVITY

Pathogen Selection

Pseudomonas syringae pv. *tomato* (Pst 50) and *Xanthomonas campestris* pv. *vesicatoria* (Xcv 46) are gram-negative bacteria both affecting tomato plants. Their sensitivity to thymol was evaluated as described below, in order to select the most sensitive pathogenic species.

A loop of each bacterial suspension was taken from the long storage cultures at 4°C and streaked on the surface of Petri dishes containing Nutrient Glucose Agar (NGA) (Nutrient Agar amended with 2.5 g/L Glucose). Plates were incubated at 27 °C for 48 hours, then bacteria were scraped from the agar surface and suspended in saline solution (NaCl 0.8 %) to prepare a suspension of optical density (OD) 0.1 at 530 nm corresponding to about $1x10^8$ colony-forming units per mL (CFU/mL). 1.5 mL of each suspension were placed in a sterile Petri dish, then 15 mL of melted NGA was added and gently mixed with the suspension. Plates were left at room temperature (RT) under a laminar flow hood to allow agar solidification, then 3 mg of solid thymol were placed in the center of the agar surface. The plates were sealed with three layers of parafilm and incubated at 27 °C for 48 hours. The antibacterial activity was evaluated by measuring the diameter (cm) of the inhibition zone between the thymol and the margin of the bacterial growth.

Determination of thymol minimum inhibitory concentration (MIC)

The next tests were performed using the pathogen Xcv that resulted the most sensitive species to thymol. Firstly, the growth of Xcv was studied in presence of increasing amount of thymol.

Aliquots of 16 µL of Xcv bacterial suspension (OD 0.1 at 530 nm, prepared as described before), were transferred into plastic tubes containing 8 mL of sterile nutrient broth (NB). Appropriate amounts of a stock solution of thymol in methanol (4 mg/mL) were added to the cultures to get final concentrations of: 100, 500, 1000 µg/mL. An evaluation of methanol toxicity to Xcv was also performed growing the bacterium in nutrient broth (NB) amended with increasing methanol concentrations (0.4%, 2%, 4%). Three replicates per each concentration were prepared. Cultures were incubated at 27 °C on a rotary shaker. Bacterial growth was monitored by reading the OD of the cultures at 530 nm after 0, 24, 48, 72 and 96 hours of incubation. A spectrophotometer Easyspec (International PBI, IT) was employed for measurements.

Inhibition of Xcv growth by the thymol-delivering nanovectors

The antibacterial activity of *Nannochloropsis*-derived and soybean phosphatidylcholine nanovectors delivering thymol, was then tested against Xcv. From the results obtained by the preliminary growth inhibition test, thymol at a concentration of 100 µg/mL showed a bactericidal effect, hence concentrations of 100, 250 and 500 µg/mL of thymol delivered via nanovectors were tested. The 100ppm aqueous solution of thymol was used as control in order to compare the effect of the pure compound with that of the delivered one.

Bacterial culture preparation and methodology to test Xcv sensitivity were the same described previously for preliminary test. Growth curves of Xcv were obtained by dilution plate count method. Samples of cultures were taken after 0, 24, 48, 72, 96 h of incubation at 27°C: 500 µL of each culture were suspended into 4.5 mL of saline solution and serially diluted. Five replicates of 20 µL per each dilution were placed on the surface of NGA in Petri dishes. Colonies were counted after 48 hours of incubation at 27 °C and final concentration was expressed as CFU/mL.

2.2.7 STATISTICAL ANALYSIS

Data from microbiological tests were not normally distributed (Kolmogorov-Smirnov one-sample test) and were therefore analyzed using the non-parametric Kruskal-Wallis rank-sum test followed by the Mann-Whitney U Test for multiple comparisons between different treatments within the same sampling time, and with the non-parametric Friedman test for comparisons within each single treatment at different sampling times. Differences were accepted when significant at the 5% level. Statistical analyses were performed using SYSTAT 12.0 software (Systat Software Inc., San Jose, CA, USA).

2.3 RESULTS AND DISCUSSION

2.3.1 EXTRACTION OF THE LIPID FRACTION FROM *NANNOCHLOROPSIS* SP.

Dry and powdered biomass of starved *Nannochloropsis* sp., i.e. grown in nitrogen-depleted medium, was employed for the lipid extraction. As reported in literature[10], the cultivation in such conditions induces the microalga to accumulate up to 68% of lipids. 730 mg of lipids were obtained from 1441 mg of dry biomass, for a yield of extraction of 50.65%.

2.3.2 *NANNOCHLOROPSIS*'S FATTY ACID COMPOSITION

The lipid composition of starved *Nannochloropsis* sp., i.e. cultivated in nitrogen-deprived growth medium, was determined and results showed a strong prevalence of neutral lipids, which account for about 76% of the total, followed by glycolipids (19.37%) and phospholipids (4.73%) (Fig. 15). This is in line with the fact that in microalgae, stress factors such as nitrogen-depleted growth conditions, induce a sharp decrease of cell replication and accumulation of neutral lipids as storage (mainly triacylglycerides, TAGs)[14]. C 16:0 and C 16:1 n 7 are typically incorporated into TAGs[15], and together with C 18:1 n 9, were found to be the most representative in neutral lipid fraction, accounting respectively for about the 25%, 18% and 24% (Table 6). The saturated C 16:0, commonly known as palmitic acid, was predominant in all the fractions, representing up to the 62% of the fatty acids in the phospholipid fraction. Apart from palmitic acid, the main constituents of the glycolipid fraction were oleic acid (C 18:1 n 9; 26%), myristic acid (C 14:0; 17%) and stearic acid (C18:0; 12%), whilst myristic acid (13%) was found to be more abundant than oleic acid (10%) in phospholipid fraction. Lower amounts of

long chain fatty acids (i.e. equal or more than 20 carbon units) accounting for an overall 8.58%, were also found in the three fractions, the most representative of which were the polyunsaturated eicosapentaenoic acid (C 20:5 n 3; 5.3%) and arachidonic acid (C20:4 n 6; 2%). Saturated fatty acids were strongly predominant in glycolipid and phospholipid fractions, whilst about the 52% of the neutral lipid fraction consisted of unsaturated fatty acids (Table 6).

Table 6. Fatty acid composition (%) of neutral lipids (NL), glycolipids (GL), and phospholipids (PL) of starved *Nannochloropsis*. sp

	Lipid class			
Fatty acid	NL fraction	GL fraction	PL fraction	TOTAL (%)
C 10:0	0.10	0.17	0.00	0.10
C 14:0	14.31	17.25	13.03	14.54
C 15:0	0.78	0.91	0.62	0.78
C 16:0	25.34	35.85	61.62	28.61
C 16:1 n 7	17.85	3.72	4.03	14.31
C 17:0	1.90	1.67	0.82	1.77
C 18:0	5.26	12.08	8.42	6.56
C 18:1 n 9 c	23.61	26.40	10.28	15.46
C 20:0	0.36	0.31	0.19	0.34
C 20:3 n 6	0.99	0.31	0.42	0.82
C 20:4 n 6	2.62	0.43	0.25	2.06
C 20:5 n 3	6.82	0.85	0.28	5.30
C 22:0	0.07	0.05	0.06	0.06
Total (%)	75.90	19.37	4.73	100.00
total saturated	48.10	68.29	84.75	
total unsaturated	51.90	31.71	15.25	

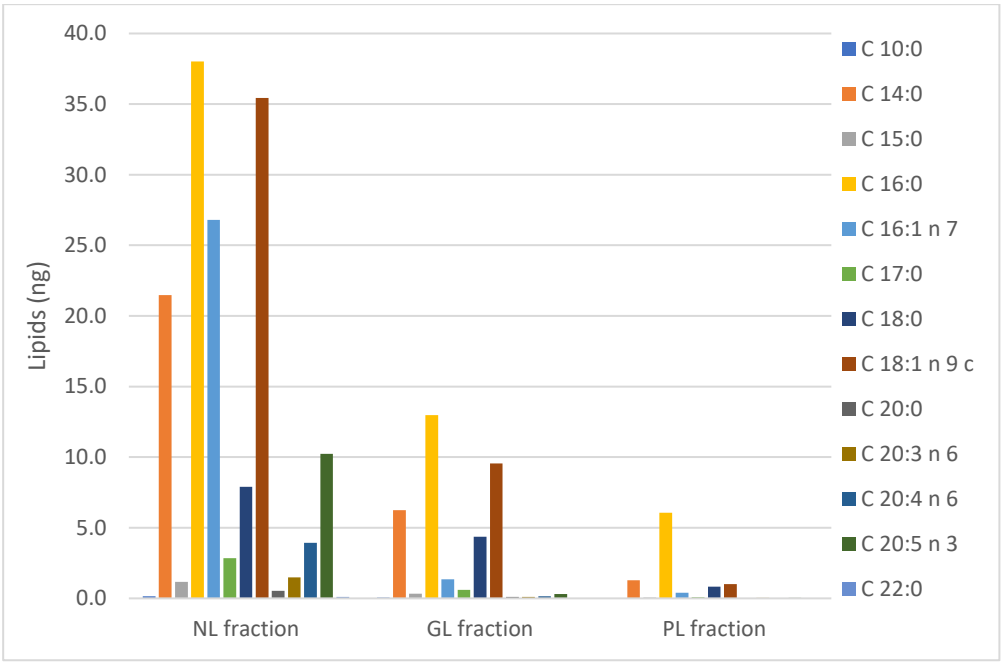

Figure 15. Fatty acid profile (ng) of neutral lipids (NL), glycolipids (GL), and phospholipids (PL) of starved *Nannochloropsis*. sp.

2.3.3 STRUCTURAL CHARACTERIZATION OF THE NANOVECTORS: DYNAMIC LIGHT SCATTERING, ZETA POTENTIAL AND SMALL ANLGE X-RAY SCATTERING

Dynamic Light Scattering measurements of plain soybean phosphatidylcholine vectors revealed the presence of a population with mean size 128 nm; a second distribution, centered at 136 nm, was also observed after thymol uploading (Fig. 16). The *Nannochloropsis*-derived nanovectors showed a mean diameter ranging from 114 for the thymol-delivering vectors, to 142 nm for the empty ones (Fig. 17). Polydispersity index (PdI) values were below 0.5, indicating a broad but defined size distribution for all the samples analyzed. From these results it is possible to infer that that thymol uploading left the structure substantially unchanged. Zeta potential measurements

showed that the surface charge was close to neutrality for all the samples, since the recorded potential values ranged between -5 ÷ +1 mV (Table 7).

Nanovectors	Mean size (nm)	PdI	Zeta potential (mV)
Plain S100-NVs	128.2	0.402	-1.03±0.95
Thymol loaded S100-NVs	136.2	0.285	+1.06±0.41
Plain N-NVs	142.2	0.332	-1.19±0.92
Thymol loaded N-NVs	113.7	0.116	-4.74±0.40

Table 7. Mean size values and Polydispersity indexes obtained by Dynamic Light Scattering measurements. Zeta potential values are also reported as mean values of ten runs ± standard error.

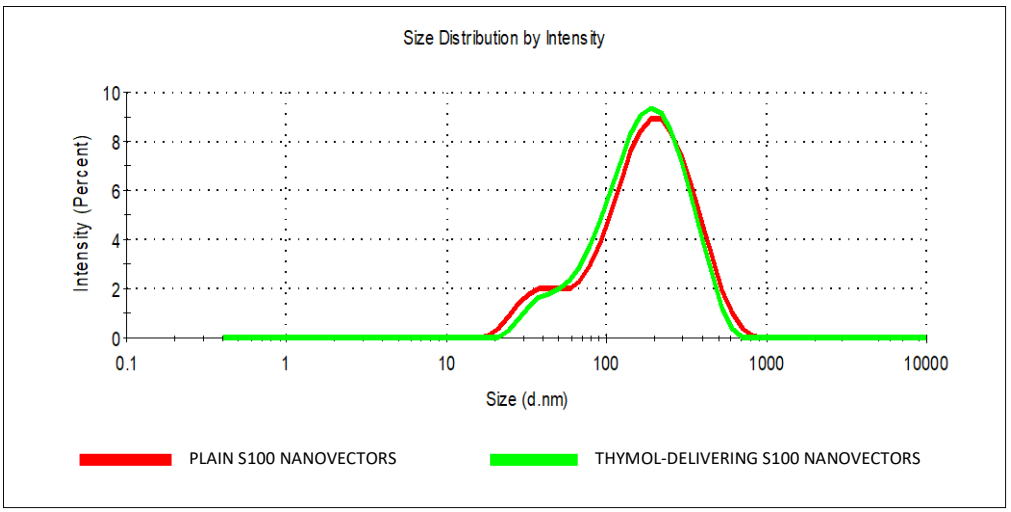

Figure 16. Dynamic light scattering intensity distributions of plain (red curve) and loaded (green curve) soybean phosphatidylcholine nanovectors (S100 NVs).

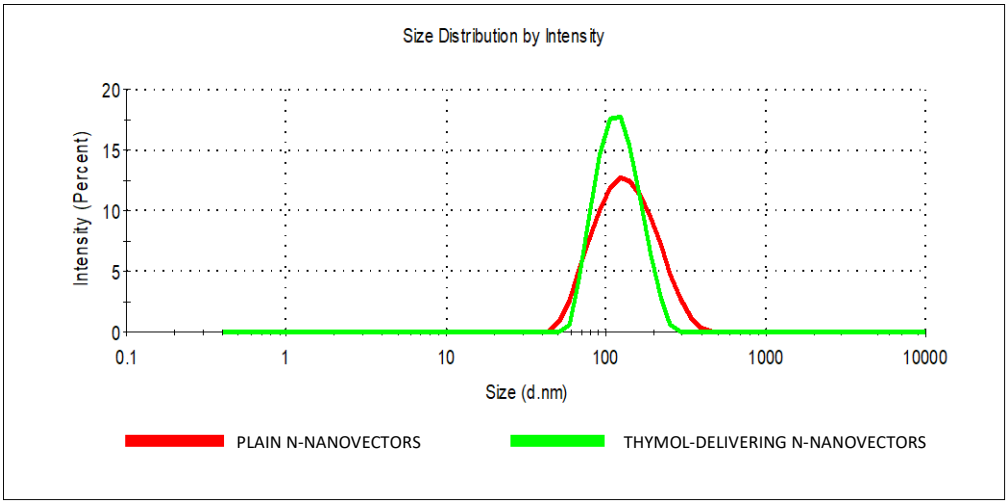

Figure 17. Dynamic light scattering intensity distributions of plain (red curve) and loaded (green curve) *Nannochloropsis*-derived nanovectors (N-NVs).

Regarding *Nannochloropsis*-derived nanovectors, Small Angle X-ray Scattering revealed the presence of clearly visible peaks whose pattern (1: √2: √6: √8: √10) could be attributed to cubic phases[16]. Therefore, a cubosome-like structure, consisting of cubic crystalline phases with an internal network of water channels, can be hypothesized for the aggregates in solution (Fig.18).

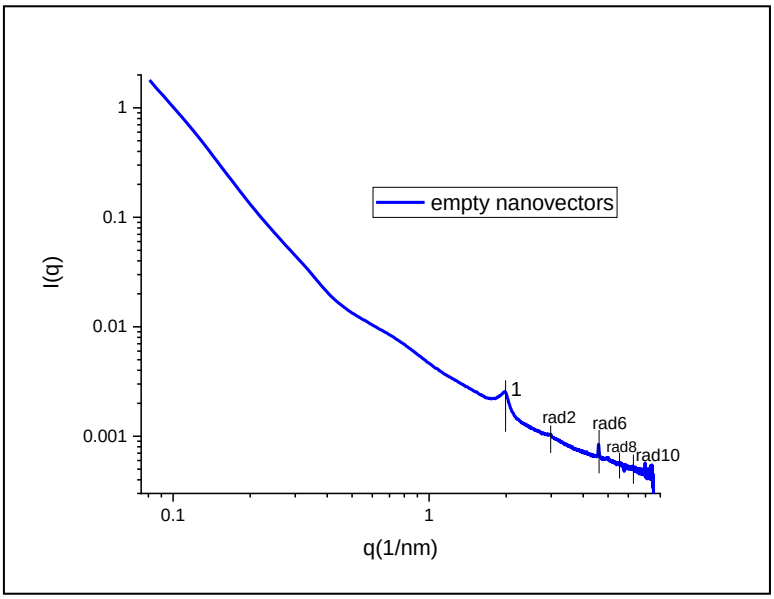

Figure 18. Small angle X-ray scattering profile of plain *Nannochloropsis*-derived nanovectors.

2.3.4 GC-MS ANALYSIS

The thymol content was measured by GC-MS analysis and results are summarized in table 8.

Nanovectors	Thymol concentration (μg/mL)	Loading efficiency (%)
N-NVs	906±117	70.4
S 100-NVs	1248±154	96.9

Table 8. Thymol concentration and loading efficiency registered for *Nannochloropsis*-derived NVs and S100-NVs. Concentrations are reported as mean values of three replicates ± standard error.

All vectors showed high loading capacity and in the case of S100 nanovectors, the GC-MS data indicated that almost all thymol could be incorporated. The differences observed were clearly related to the different lipid composition of the two systems. Soybean phosphatidylcholine is widely employed in the manufacturing of liposomes[17]: the use of this purified phospholipid mixture eases the development of ordered structures displaying both hydrophobic and hydrophilic character. Therefore thymol, which is lipid-soluble but also slightly soluble in water, is expected to well associate with this type of nanocarriers, as confirmed by the high loading rate registered. On the other hand, the lower loading efficiency showed by the *Nannochloropsis*-derived nanovectors was consistent with the heterogeneous composition of this nanosystem, in which the three main classes of zwitterionic lipids, glycolipids and phospholipids were all present. The lipid extract combined with a 15% of pure DOPE was used to develop carriers in which, despite the complex composition, thymol was uploaded with an efficiency of about 70%.

2.3.5 BACTERIAL GROWTH INHIBITION TEST

Pathogen selection

The bacteria *Xanthomonas campestris* pv. *vesicatoria* (Xcv) and *Pseudomonas syringe* pv. *tomato* (Pst) are phytopathogens of tomato plant and their sensitivity to thymol was evaluated *in vitro*, measuring the size of the growth inhibition halo, which reflects the susceptibility of the microorganism to the tested compound (Fig. 20). The mean growth inhibition diameter measured for Xcv was significantly higher than the value registered for Pst (respectively 4.8 cm and 1.9 cm) (Fig. 19), then Xcv was chosen as the target bacterium for an in-depth investigation of its response to the thymol-delivering nanovectors.

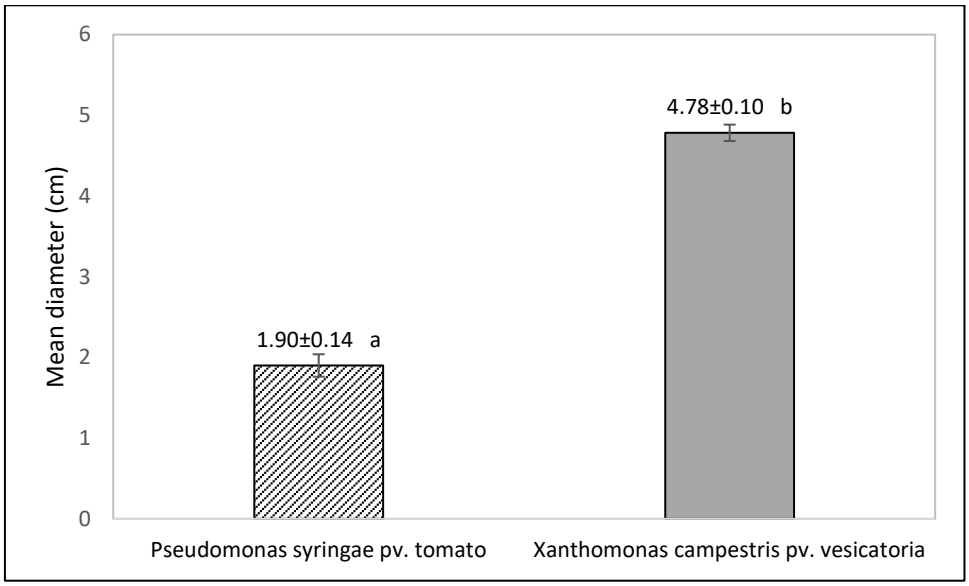

Figure 19. Growth inhibition halos (mean diameter ± standard error) generated by thymol against *Pseudomonas syringae* pv. *tomato* and *Xanthomonas campestris* pv. *vesicatoria*. Different letters indicate a significant difference by Mann-Withney U test (p-value=0.004; χ^2=8.456, d.f.=1).

Figure 20. Pathogen selection test. Inhibition halos are marked by dashed lines: *Pseudomonas syringae* pv. *tomato* (right Petri dish) and *Xanthomonas campestris* pv. *vesicatoria* (left Petri dish) inhibited by thymol.

Determination of thymol minimum inhibitory concentration (MIC)

Before testing nanovectors' toxicity, a preliminary test was performed growing the bacterium Xcv in presence of 1000, 500 and 100 ppm thymol concentrations (Fig. 21 A and B). A stock solution of thymol dissolved in methanol was employed for the test, therefore a parallel evaluation of the solvent toxicity was also performed.

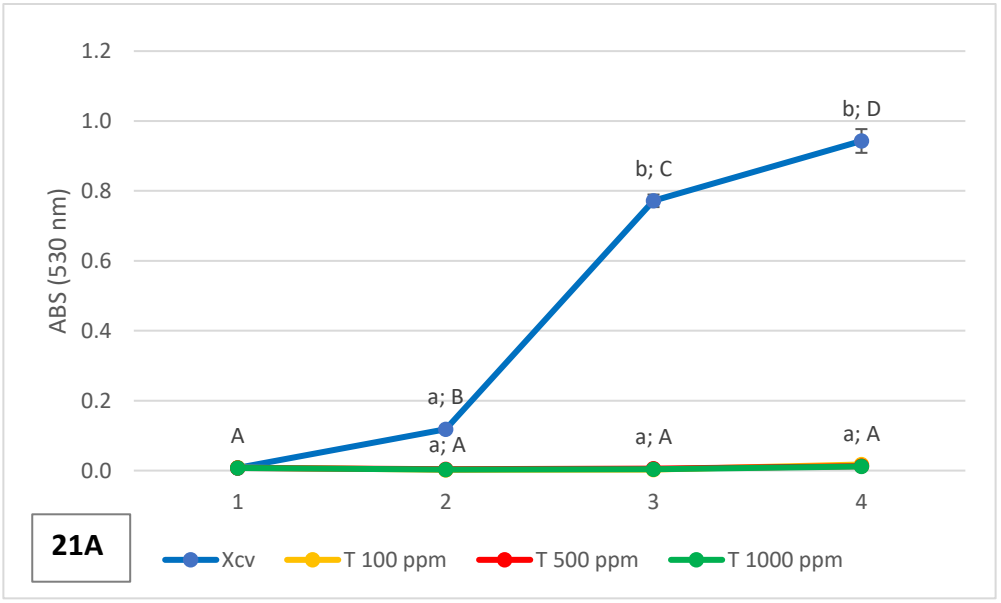

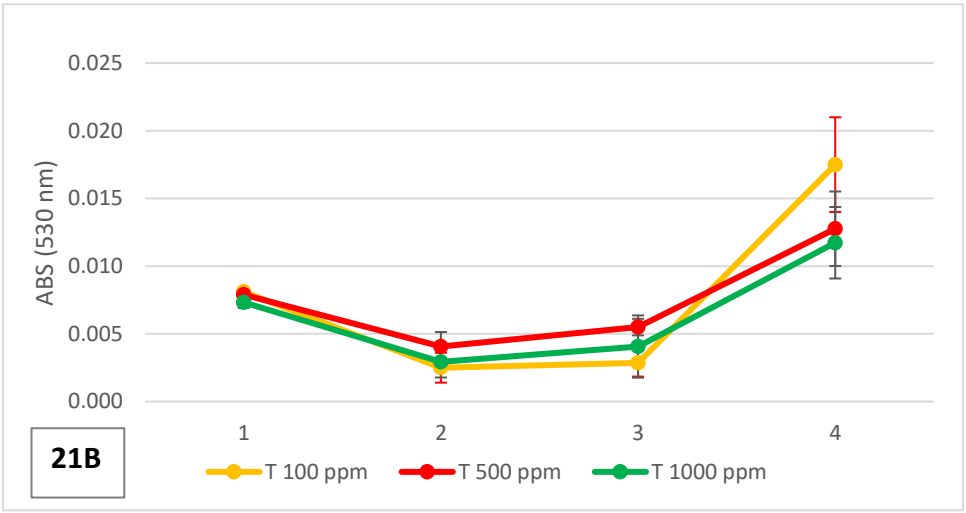

Figure 21. Preliminary growth inhibition test: growth curves of Xcv grown in presence of thymol (100, 500, 1000 ppm) and control, determined by Optical Density readings at 530 nm, after 0, 24, 48, 72 hours of incubation. Details of the overlapping curves are clarified in the graph B. Different letters indicate significant differences (p<0.05). Lowercase letters refer to the comparison between different treatments by non-parametric Mann-Whitney U Test (d.f.=3, N° samples=12, a<b). Uppercase letters refer to the analysis between different sampling time (d.f.=3, N° samples=12, A<B<C<D) within each single treatment by non-parametric Friedman test.

After 24 hours of incubation, the treatments tested (T 100 ppm, T 500 ppm and T 1000 ppm) completely shot down the growth of the bacterium and no growth was observed after 48 and 72 hours. Even the lower concentration tested (100 ppm) was found to be bactericidal against Xcv, whilst a regular growth curve was obtained for control (Xcv), with little cell division till 24 hours sampling time (lag phase), followed by exponential growth (log phase, 24-48 hours) and finally a gradual growth decrease (beginning of the stationary phase, starting from 48 hours).

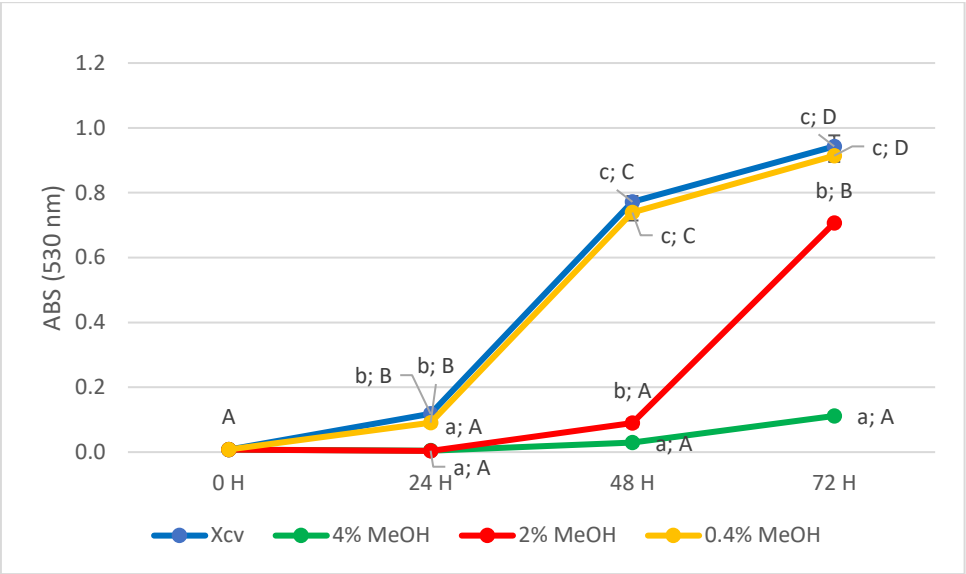

Figure 22. Determination of thymol minimum inhibitory concentration (MIC): growth curves of Xcv grown in presence of methanol (0.4%, 2%, 4%) and control, determined by OD readings at 530 nm, after 0, 24, 48, 72 hours of incubation. Different letters indicate significant differences (p<0.05). Lowercase letters refer to the comparison between different treatments by non-parametric Mann-Whitney U Test (d.f.=3, N° samples=12, a<b<c). Uppercase letters refer to the analysis between different sampling time (d.f.=3, N° samples=12, A<B<C<D) within each single treatment by non-parametric Friedman test.

At the lower methanol concentration tested (0.4%), no inhibitory effect on Xcv's growth was observed. In fact, 0.4% MeOH curve overlaps growth curve of Xcv and no significant differences were registered between treatment and control. Since this amount of methanol was used to get a final thymol concentration of 100 ppm, the bactericidal effect against Xcv, can be ascribed to the activity of thymol. Significative differences between control and higher methanol concentrations (2% and 4%) were found at 24, 48 and 72-hours sampling times (Fig. 22).

Inhibition of Xcv's growth by the thymol-delivering nanovectors

Since the 100 ppm concentration of pure thymol resulted inhibitory to Xcv, the effect of thymol 100 ppm delivered through nanovectors on the bacterium growth curve was investigated. The aqueous solution of pure thymol 100 ppm was used as control (Fig. 23). Both *Nannochloropsis*-derived and soybean phosphatidylcholine nanovectors reduced the bacterial growth by an order of magnitude and statistically significant differences were observed between these treatments and control (Xcv), at all sampling times. A statistically significant reduction of the growth was also observed between thymol 100 ppm in water solution and control at 48, 72 and 96 hours. Concerning the comparison between thymol delivered via nanovectors (NT100 ppm and S100T 100ppm) and thymol in water solution (T100 in W), statistically significant differences were registered at 24, 48, 72 and 96 hours, with no growth observed for T100 in W treatment. Hence, at the tested concentration of 100 ppm, the treatment T100 in W resulted the most effective. The lower efficacy of the thymol-delivering nanovectors could be due to the gradual release of the antibacterial compound from the carriers. Therefore, higher concentrations could be necessary to get the same effect as T100 in W, to break down the bacterial growth. The successive toxicity assay was then carried out testing the effect of nanovectors delivering thymol 100, 250 and 500 ppm (Fig. 24). Since the treatment with *Nannochloropis*-derived nanovectors delivering thymol 100 ppm was not significantly different from that with soybean phosphatidylcoline nanovectors, the successive experiment was performed testing the effect of the only *Nannochloropis*-derived ones.

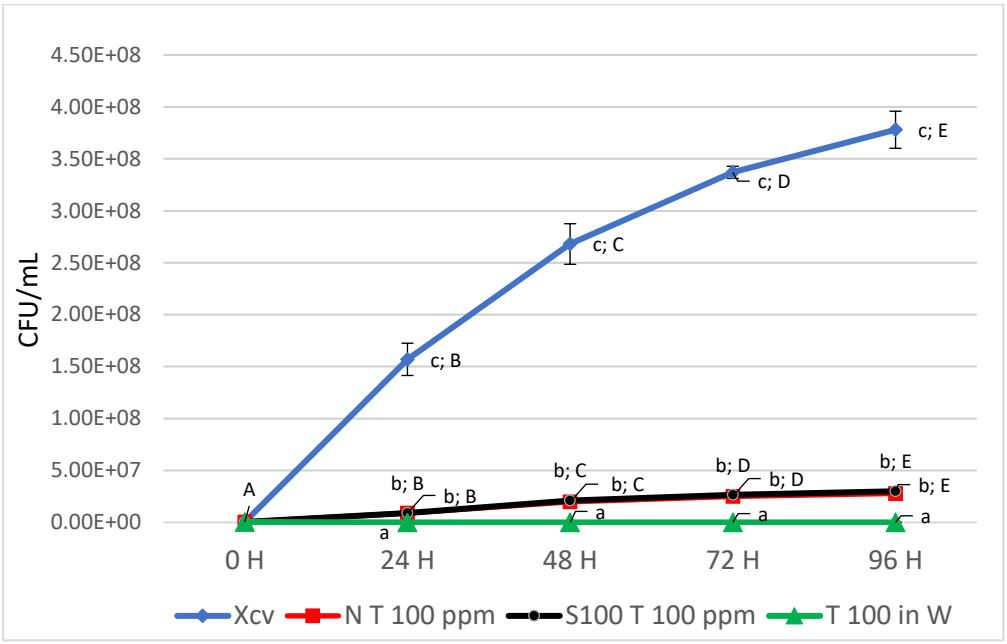

Figure 23. Effect of thymol 100 ppm in water solution and delivered via nanovectors (NT 100 ppm, S100 T 100ppm) on Xcv's growth. Growth curves were obtained by serial colony counts after 0, 24, 48, 72 and 96 hours from inoculation. Different letters indicate significant differences (p<0.05). Lowercase letters refer to the comparison between different treatments by non-parametric Mann-Whitney U Test (d.f.=3, N° samples=12, a<b<c). Uppercase letters refer to the analysis between different sampling time (d.f.=3, N° samples=12, A<B<C<D<E) within each single treatment by non-parametric Friedman test.

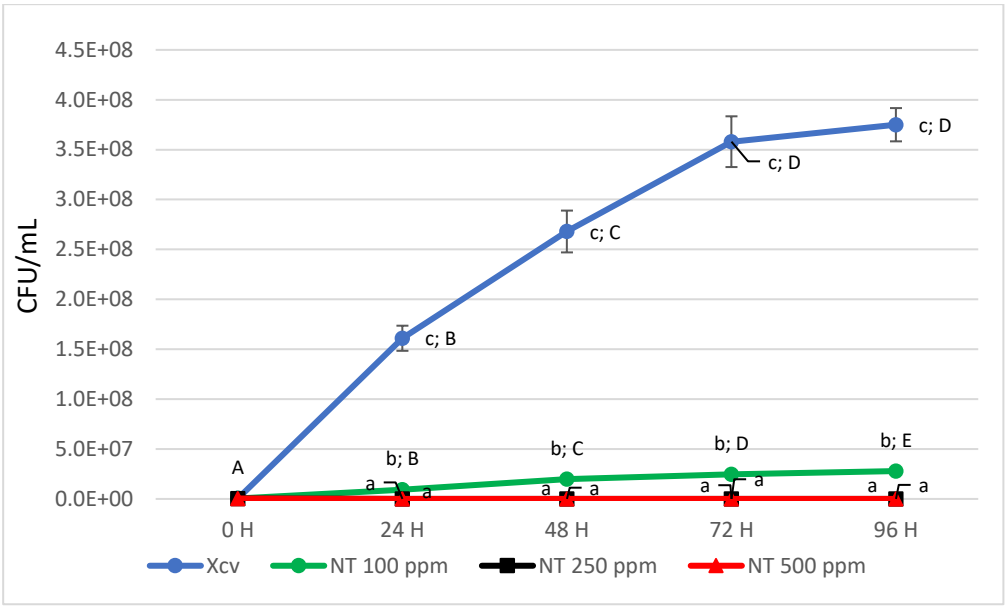

Figure 24. Effect of thymol 100 ppm, 250ppm and 500 ppm delivered through *Nannochloropsis*-derived nanovectors (NT) on Xcv's growth. Growth curves were obtained by serial colony counts after 0, 24, 48, 72 and 96 hours from inoculation. Different letters indicate significant differences (p<0.05). Lowercase letters refer to the comparison between different treatments by non-parametric Mann-Whitney U Test (d.f.=3, N° samples=12, a<b<c). Uppercase letters refer to the analysis between different sampling time (d.f.=3, N° samples=12, A<B<C<D<E) within each single treatment by non-parametric Friedman test.

The concentration of thymol 100 ppm loaded in *Nannochloropsis*-derived nanovectors confirmed the previously registered result, reducing Xcv's growing by an order of magnitude with significant differences between the NT 100 ppm treatment and control, at 24, 48, 72 and 96 hours. Both the highest thymol concentrations tested, 250 and 500 ppm, had a bactericidal effect, the growth of the bacteria being set to zero. No significant differences were observed within the single treatment NT 250 ppm and NT 500 ppm, pointing out the strong bioactivity of these treatments displayed since time zero. This test confirmed the hypothesis according to which 100 ppm of the pure compound had a bactericidal effect against Xcv but higher

concentrations could be necessary to get the same effect for thymol delivered through nanovectors. This is reasonably attributable to a gradual release of thymol from the nanosystem, consequently reducing the number of active molecules promptly available in solution. The antimicrobial efficacy of highly volatile compounds, like thymol, can be enhanced delaying in somehow the volatility process, therefore in this sense, the lipid-nanovectors developed in this study represent a useful tool to be further investigated.

2.4 CONCLUSIONS

In this project two sets of lipid-based nanovectors were created employing respectively soybean phosphatidylcholine and the autotrophic microalga *Nannochloropsis* sp. as starting material for the manufacturing. The final purpose was to obtain the delivery of thymol via nanovectors, since the antibacterial effectiveness of this compound is strongly affected by its high volatility. The vectors were therefore designed aiming to get a gradual release of thymol, and a consequent improvement of its long-term efficacy. Both the typologies of nanovectors displayed good thymol loading rate (i.e. >70%) and biocidal activity *in vitro* against a phytopathogenic bacterium. Hence, these preliminary results represent a promising starting point for an in-depth investigation of this nanosystem's potentialities, as a bioactive formulation alternative to the conventional ones.

2.5 REFERENCES

[1] Hossain, L., Rahman, R., & Khan, M. S. (2017). Alternatives of pesticides. In Pesticide residue in foods (pp. 147-165). Springer, Cham.

[2] Ultee, A., Bennik, M. H. J., & Moezelaar, R. (2002). The phenolic hydroxyl group of carvacrol is essential for action against the food-borne pathogen Bacillus cereus. Appl. Environ. Microbiol., 68(4), 1561-1568

[3] Dadasoglu, F., Aydin, T., Kotan, R., Cakir, A., Ozer, H., Kordali, S., ... & Mete, E. (2011). Antibacterial activities of extracts and essential oils of three Origanum species against plant pathogenic bacteria and their potential use as seed disinfectants. Journal of Plant Pathology, 271-282.

[4] Elshafie, H. S., Gruľová, D., Baranová, B., Caputo, L., De Martino, L., Sedlák, V., ... & De Feo, V. (2019). Antimicrobial activity and chemical composition of essential oil extracted from Solidago canadensis L. growing wild in Slovakia. Molecules, 24(7), 1206.

[5] Singh, B., & Sharma, R. A. (2015). Plant terpenes: defense responses, phylogenetic analysis, regulation and clinical applications. 3 Biotech, 5(2), 129-151.

[6] Madni, A., Sarfraz, M., Rehman, M., Ahmad, M., Akhtar, N., Ahmad, S., ... & Löbenberg, R. (2014). Liposomal drug delivery: a versatile platform for challenging clinical applications. Journal of Pharmacy & Pharmaceutical Sciences, 17(3), 401-426.

[7] Veldhuizen, E. J., Tjeerdsma-van Bokhoven, J. L., Zweijtzer, C., Burt, S. A., & Haagsman, H. P. (2006). Structural requirements for the antimicrobial activity of carvacrol. Journal of agricultural and Food Chemistry, 54(5), 1874-1879.

[8] Jyoti, D. D., Singh, D., Kumar, G., Karnatak, M., Chandra, S., Verma, V. P., & Shankar, R. Thymol Chemistry: A Medicinal Toolbox.

[9] Meeran, N., Fizur, M., Javed, H., Al Taee, H., Azimullah, S., & Ojha, S. K. (2017). Pharmacological properties and molecular mechanisms of thymol: prospects for its therapeutic potential and pharmaceutical development. Frontiers in pharmacology, 8, 380.

[10] Bondioli, P., Della Bella, L., Rivolta, G., Zittelli, G. C., Bassi, N., Rodolfi, L., ... & Tredici, M. R. (2012). Oil production by the marine microalgae Nannochloropsis sp. F&M-M24 and Tetraselmis suecica F&M-M33. Bioresource technology, 114, 567-572.

[11] Bonas, U., Schulte, R., Fenselau, S., Minsavage, G. V., Staskawicz, B. J., & Stall, R. E. (1991). Isolation of a gene cluster from Xanthomonas campestris pv. vesicatoria that determines pathogenicity and the hypersensitive response on pepper and tomato. Mol. Plant-Microbe Interact, 4(1), 81-88.

[12] Flemming, C. A., & Trevors, J. T. (1989). Copper toxicity and chemistry in the environment: a review. Water, Air, and Soil Pollution, 44(1-2), 143-158.

[13] Mirik, M., Aysan, Y., & Cinar, O. (2007). Copper-resistant strains of Xanthomonas axonopodis pv. vesicatoria (Doidge) Dye in the eastern Mediterranean region of turkey. Journal of Plant Pathology, 89(1), 153-154.

[14] Huerlimann, R., De Nys, R., & Heimann, K. (2010). Growth, lipid content, productivity, and fatty acid composition of tropical microalgae for scale-up production. *Biotechnology and bioengineering*, *107*(2), 245-257.

[15] Hulatt, C. J., Wijffels, R. H., Bolla, S., & Kiron, V. (2017). Production of fatty acids and protein by Nannochloropsis in flat-plate photobioreactors. *PloS one*, *12*(1), e0170440.

[16] Glatter, O. (2018). *Scattering Methods and their Application in Colloid and Interface Science*. Elsevier.

[17] Puri, A., Loomis, K., Smith, B., Lee, J. H., Yavlovich, A., Heldman, E., & Blumenthal, R. (2009). Lipid-based nanoparticles as pharmaceutical drug carriers: from concepts to clinic. *Critical Reviews™ in Therapeutic Drug Carrier Systems*, *26*(6).

SECTION 3. CO-CRYSTALS AS ANTIMICROBIAL FORMULATION DELIVERING THYMOL, EUGENOL AND CARVACROL

3.1 INTRODUCTION

Worldwide pesticide consumption is attested around 2 million tons per year, with Europe accounting for the 45% of the total amount, followed by the United States (25%) and the rest of the world (30%)[1]. The massive use of these phytochemicals is strictly related to the control of plant pathologies and pests, which is normally obtained through repeated chemical treatments, with a progressive accumulation of toxic residues in soil and water[2]. This implies serious consequences both on the environment and on human health, and claims for the introduction of safer and more sustainable techniques[3]. In this context, a new class of natural pesticides based on co-crystallization of essential oil constituents (EOCs) has been designed and experimented in this project. EOCs are secondary metabolites produced by plants and their antibacterial, antifungal and insecticide properties[4] are very well known. Terpenes and terpenoids are the main EOCs: they are typically characterized by poor water solubility, high volatility and low melting point, as most of them are liquid at room temperature. This strongly limits their application in plant protection; therefore the development of alternative formulations is needed for their employment as natural agrochemicals[5]. For instance, in the second section of this thesis, a lipid-based formulation in liquid form, specifically designed for the delivery of thymol as EO constituent, was presented. Here, co-crystallization was chosen to obtain a powdery formulation, in order to better regulate the physico-chemical properties of EOCs. Co-crystals are multicomponent crystalline materials made by different chemical entities in

a specific stoichiometric ratio and their design requires a thorough knowledge of the molecular affinity between the partner compounds involved in the synthesis. Appropriate interactions between the EOCs molecules and suitable partners should provide a robust intermolecular network for the EOCs, thus stabilizing the liquid ingredient in a solid form[6,7]. This is a relevant aspect to be taken into account, since liquid or low melting compounds are generally less chemically stable than their solid analogues[8], therefore their handling, transportation and storage present considerable environmental and cost-related challenges. Co-crystals are mainly referred in literature as crystalline materials synthesized from solid reagents, with the only exception of few papers reporting the use of liquid components[8,9]. In this work, a set of six co-crystals designed by combining eugenol (EUG; liquid), carvacrol (CAR; liquid) and thymol (THY; solid) with the two coformers phenazine (PHE) and hexamethylenetetramine (HMT), was obtained, as graphically represented in figure 25. The aim was scanning the range of properties resulted by pairing each EOC with a different molecular partner (i.e. the conformer). THY, CAR and EUG may be considered prototypal EOCs, due to their chemical structure, their widespread employment, and their known bioactivity against bacteria and fungi[10]. THY and CAR allowed to test the effect of molecular isomerism on the investigated properties, whereas EUG possesses a lipophilic chain, which possibly affects the molecular interaction with the coformer. Noteworthy, being phenol-derivatives, they all display a hydroxyl group in the structure that can act as hydrogen-bond donor. The two coformers PHE and HMT were selected as rigid molecules containing nitrogen atoms prone to act as H-bond acceptors. Initially, vanillin (VAN), theobromine (THE) and riboflavin (RIB) were also considered as potential coformers, as the first step

of the co-crystal design was the evaluation of the coformers' propensity to generate co-crystals with the selected EOCs. This was assessed calculating the hydrogen bond propensity (HBP) for each possible molecule combination (i.e. coformer/EOC; coformer/conformer; EOC/EOC), obtaining a final Multi-Component score (MC score = Best HBP heteromeric interaction – best HBP homomeric interaction) which indicates a favored co-crystal formation if positive, whilst negative values correspond to unfavored interactions (so co-crystallization in unlikely to occur).

In the case of VAN, THE and RIB, the HBP analysis suggested that homomeric interactions would have prevailed with respect to heteromeric interactions with THY, CAR and EUG; accordingly, co-crystallization experiments failed. On the contrary, positive MC scores were obtained for PHE and HMT combined with the three EOCs and the six resulting co-crystals were indeed successfully synthesized. The co-crystals were then characterized in terms of structure, physical properties and *in vitro* biological activity. Their performances were also compared with those of the corresponding pure EOCs (i.e. thymol, carvacrol and eugenol). The synthetic procedure adopted for the preparation was solvent-free[11,12], thus reducing costs and preventing environmental contamination from solvent disposal. An example of the detailed structure of HMT-THY co-crystal is reported in figure 26.

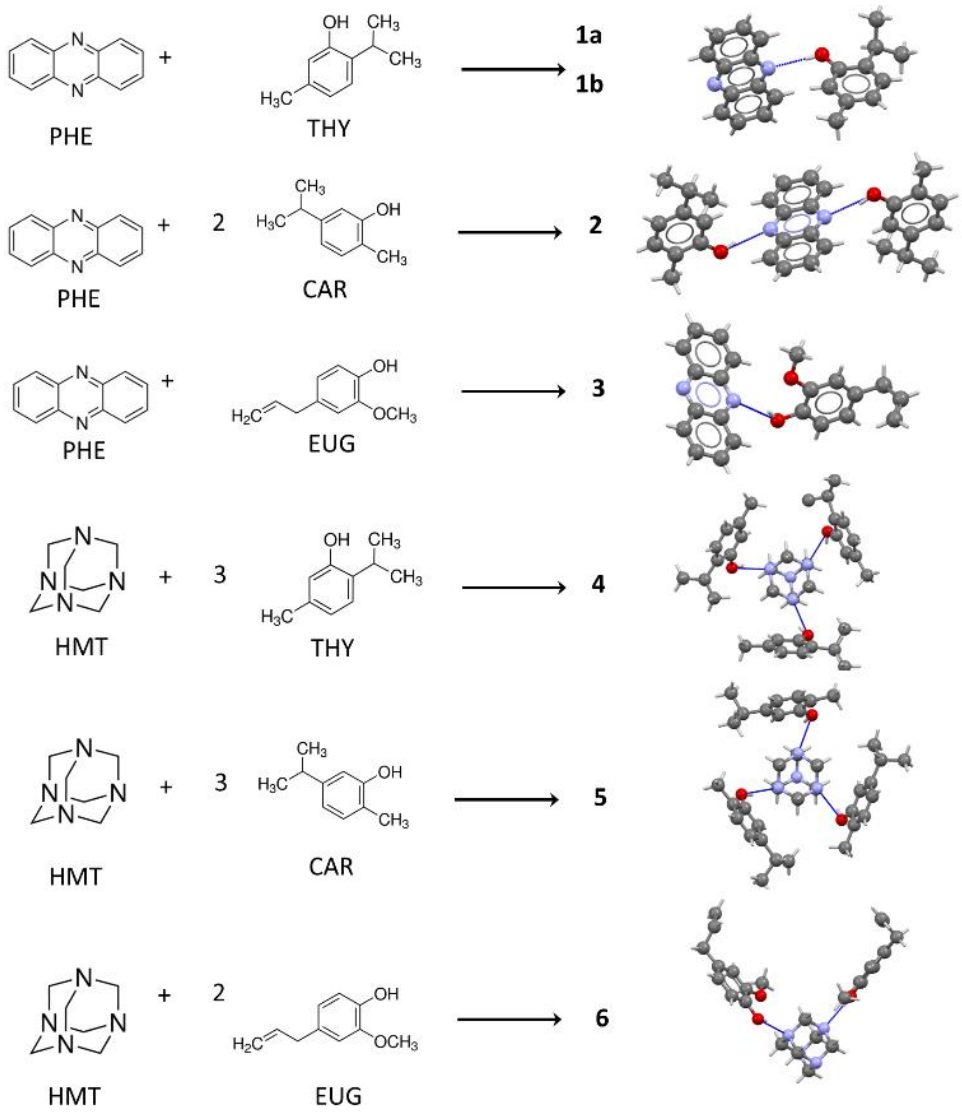

Figure 25. Schematic representation of the co-crystals **1a**-**6** synthesized from the combination of three essential oil constituents (THY=Thymol, CAR=Carvacrol and EUG=Eugenol) and two coformers (PHE=Phenazine and HMT=Hexamethylenetetramine). Thumbnail images of the corresponding crystalline structures showing each EOC-coformer association. All not-H atoms are reported in ball-and-stick style. Colour code: C=grey, N=blue, O=red. Hydrogen atoms are reported in capped stick style for clarity. Blue dotted lines represent the EOC-coformer intermolecular H-bonds.

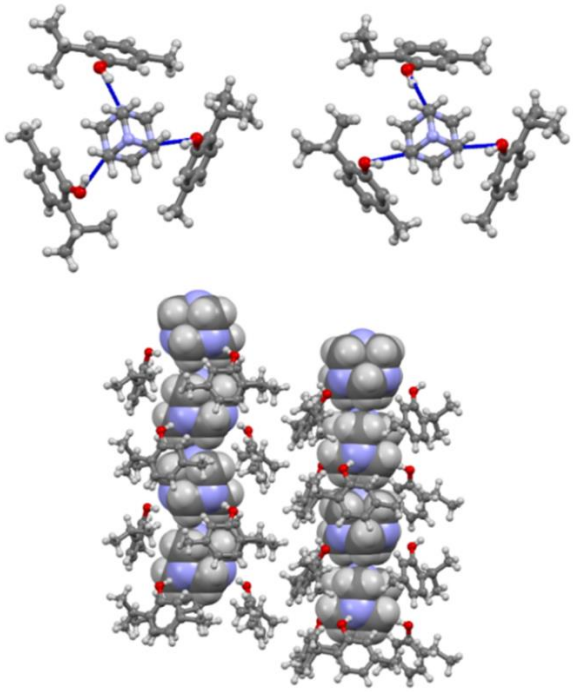

Figure 26. Tridimensional structure of HMT-THY co-crystal (molar ratio 1:3). Upper part of the image showing HMT:THY_3 tetramers, with three thymol molecules organized around a central HMT. Lower part of the image showing arrays of THY trimers arranged in an antiparallel fashion: clockwise and anticlockwise tetramers are alternated within each array.

3.2 MATERIALS AND METHODS

3.2.1 SYNTHESIS OF CO-CRYSTALS

Co-crystal 1a-6 were all prepared by grinding or direct mixing methods, with no need of any solvent addition.

Since most of the resulting co-crystals are characterized by low melting point, the mortars containing samples were placed at low temperature (4°C) to prevent melting of the product due to heating by mechanic friction. Once thermalized back at ambient temperature, powder samples were collected in closed vials.

The main characteristics of the six co-crystals are summarized in table 9.

Table 9. Detailed composition of co-crystals **1a-6**.

Co-crystal	Ref. number	Coformer (mg)	EOCs	Molar ratio	Aspect
PHE-THY	1a; 1b	180	154 mg	1:1	Whitish powder
PHE-CAR	2	180	320 µL	1:2	Plate-like yellowish crystals
PHE-EUG	3	180	328 µL	1:1	Needle-like yellowish crystals
HMT-THY	4	154	450 mg	1:3	Needle-like crystals
HMT-CAR	5	154	450 µL	1:3	Plate-like crystals
HMT-EUG	6	154	320 µL	1:2	Needle-like crystals

3.2.2 PHYSICO-CHEMICAL CHARACTERIZATION

HEADSPACE-GC/MS ANALYSES

THY, CAR, EUG and co-crystals **1a**-**6** (1 mg) were independently inserted into 10 mL vials and maintained at RT and 4°C, respectively for 5 min, 3, 7 and 14 days. One mL of the headspace above the sample was injected into the gas chromatograph by using a PAL COMBI-xt autosampler (CTC Analytics AG, Zwingen, Switzerland). Three independent replicated measurements were always performed. A HP 6890 Series Plus gas chromatograph (Agilent Technologies, Palo Alto, CA) equipped with a MSD 5973 mass spectrometer (Agilent Technologies) was used. Helium was used as the carrier gas at a constant flow of 1.3 mL/min. Chromatographic analysis was performed on a 30 m × 0.25 mm, df 0.25 µm MDN-5S capillary column (Supelco, Bellerofonte, USA), using the following temperature programme: initial temperature 70°C, 10°C/min up to 140°C, 5°C/min up to 170°C.

The transfer line and source were maintained at the temperatures of 270 and 150 °C, respectively. Full scan electron ionization (EI) data were acquired under the following conditions: ionization energy: 70 eV; mass range: 40-200 amu; scan time: 3 scan/s; electron multiplier voltage: 2212 V. Signal

acquisition and data handling were performed using the HP Chemstation (Agilent Technologies). Data collected were evaluated by using the statistical package SPSS Statistics (IBM, Milan, Italy).

SOLUBILITY TEST IN WATER

Solubility test in water was performed according to the flask method described in the OECD test guideline 105[13].

3.2.3 ANTIMICROBIAL ACTIVITY OF CO-CRYSTALS

MICROBIAL CULTURES

The antimicrobial activity of co-crystals was evaluated against different species of bacteria and fungi that were selected from the microbial collection of IPSP-CNR. Tests were performed against the gram-negative bacteria *Agrobacterium tumefaciens* (At C58), *Pseudomonas syringae* pv. *tomato* (Pst 50), *Xanthomonas arboricola* pv. *pruni* (Xap Lc), the gram-positive bacteria *Bacillus amyloliquefaciens* (Ba M123), *Clavibacter michiganensis* subsp. *michiganensis* (Cmm), *Rhodococcus fascians* (Rf LMG 3605) and the fungi *Alternaria alternata* (Aa), *Fusarium oxysporum* f.sp. *lycopersici* (Fol) and *Pythium ultimum* (Pu). All strains, except for *B. amyloliquefaciens*, are phytopathogenic species.

The following treatments were considered for antimicrobial assays: the pure three EOCs (CAR, EUG and THY), the six co-crystals (1a-6), PHE, HMT, and sterilized distilled water (SDW) as control. All tests were performed in triplicates or quadruplicates.

ANTIBACTERIAL ACTIVITY

Strains were grown in nutrient agar amended with 0.25% glucose (NGA) for 48 hours. The bacterial cultures were used to prepare suspensions in saline solution (SS 0.8% NaCl) of OD 0.1 at 530 nm corresponding to about $1x10^8$ cfu/mL. 1.5 mL of the suspensions were placed on the bottom of a sterile Petri dish where 15 mL of NGA were added and gently mixed with the suspension. Plates were left at room temperature under a laminar hood flux to allow agar solidification and then a sterile filter paper disk of 0.5 cm diameter was placed in the center of the agar surface. 20 mg of each co-crystal, 15 mg of each pure EOC, 10 mg of PHE and 6 mg of HMT were placed on the paper disk and then the plates were sealed with three layers of parafilm and incubated at 25±2 °C for 24-48 hours. The antibacterial activity was evaluated by measuring the width of the inhibition halo surrounding the paper disk.

ANTIFUNGAL ACTIVITY

All fungal strains were grown on potato dextrose agar medium (PDA) at 24±2 °C for a time length suitable for the different species. *A. alternata* and *F. o.* f.sp. *lycopersici* produced *in vitro* high number of conidia and for these two species a conidial suspension was prepared. A volume of 10 mL of SS was added to the plate containing the fungal culture and the conidia were scraped from the colony surface by using a sterile spatula. The concentration of suspension was determined by counting the conidia using a Burker chamber and adjusted to a final concentration of $1x10^5$ conidia/mL. 1.5 mL of the suspensions were placed on the bottom of a sterile Petri dish where 15 mL of PDA were poured and gently mixed with the suspension. From this step, the procedure followed that previously described for bacteria.

The fungus *P. ultimum* did not produce conidia, so that a different protocol was used. Disks of 0.5 cm diameter were cut from the edge of the fungal colony grown on PDA medium and placed on the surface of new PDA at one cm from the plate border. At the opposite site a sterile paper disk of 0.5 cm diameter was disposed and 20 mg of the compound to be tested were placed on the disk surface. Plates were incubated at 24±2 °C for 48-72 h. The antifungal activity was evaluated by measuring the width of the inhibition halo formed between the margin of the fungal colony and the paper disk.

STATISTICAL ANALYSIS

In order to investigate the efficacy of co-crystals compared to their chemical entities, the inhibitory effect on the growth of microorganism was calculated and compared within each treatment combination: EOC, its co-crystal, the molecular coformer and SDW. Besides, variation in microorganism response against each single treatment was determined and compared within bacterial species and within fungal species. Data were not normally distributed (Kolmogorov-Smirnov one-sample test) and they were analyzed using the non-parametric Kruskal-Wallis rank-sum test followed by the Mann-Whitney U Test for multiple comparisons. Differences were accepted when significant at the 5% level. Statistical analyses were performed using SYSTAT 12.0 software (Systat Software Inc., San Jose, CA, USA).

3.3 RESULTS AND DISCUSSION

A detailed characterization of the crystalline structure of the six co-crystals was provided by the Department of Chemistry, Life Sciences and Environmental Sustainability of the University of Parma. Physical parameters, such as melting point (MP) and release energy values, were also determined and reported for completeness in table 10.

Results obtained about other physical parameters, such as water solubility and EOCs release, and about the bioactivity displayed by co-crystals are here presented and discussed in the following paragraphs.

3.3.2 PHYSICAL PROPERTIES OF CO-CRYSTALS

Co-crystals were fully characterized in terms of EOCs release and water solubility. Analyses were performed at different temperatures to test the co-crystals' adaptivity to varying external conditions. Results obtained are summarized in Table 10.

Co-crystal	MP	Release energy	Water Solubility		EOs release 30°C (%)		EOs release 4°C (%)	
	(°C)	(kJ/mol)	30°C	4 °C	5 (min)	14 (days)	5 (min)	14 (days)
1a	87.3	-79.75	ns	ns	63	30	19	24
1b	90	-83,45	-	-	-	-	-	-
2	53.1	-83.4	ns	ns	52	25	6	6
3	38.8	-89.65	ns	ns	30	24	0	0
4	42.6	-79.9	ns	ns	61	14	4	4
5	33	-80.65	-	s	-	-	5	4
6	85.1	-99.8	s	s	29	0	0	0

Table 10. Physical properties of co-crystals **1a-6**. Melting point (MP) of starting materials are THY_{mp}=49°C, CAR_{mp}=1°C, EUG_{mp}=-30°C. Release Energy calculated at B3LYP/6-31G (d, p) level of theory. Solubility in water observed at 20 g/L (ns= non-soluble, s=soluble); same results were observed both after 5 min and 72h. EOCs release in the headspace after 5 minutes and 14 days, normalized to the pure EOCs acute release. Properties of **1b** were not tested as it is an elusive polymorph. Water solubility and EOC-release of **5** was not tested at 30 °C because of its low melting temperature.

RELEASE OF EOCs FROM CO-CRYSTALS

In the food industry, EOCs are used as food flavorings whilst their employment as food preservatives[14] is still very limited due to their high volatility. Therefore, co-crystallization has been investigated as mean to tune EOCs' volatility.

Each co-crystal was tested in terms of EOC release by performing headspace-gas chromatography/mass spectrometry (HS-GC/MS) analyses over a period of 14 days. Results were then compared with those of the pure EOCs. As expected, pure EOCs showed a noticeable decrease in the responses of the active component at room temperature, until complete disappearance of the GC responses after 14 days (Fig. 27, left column, plain line). Co-crystallization significantly alters the delivery profile of the active component both in terms of acute and prolonged release (Fig. 27, left column, dashed and dotted lines). If compared with the pure substances, the acute EOC release resulted significantly limited for co-crystals (about 60% for **1a** and **4**, 50% for **2** and 30% for **3** and **6**; table 10). Moreover, the co-crystal release profile over 14 days is significantly more persistent, thus suggesting that co-crystallization plays an important role for a controlled release of the active component. Noteworthy, the release profile is extremely influenced by the coformer used: HMT-based co-crystals (**4** and **6**) showed a lower EOCs release with respect to their PHE-based analogues (**1a** and **3**). Since EOCs are also used as food preservatives for perishable products such as tubers or vegetables, often stored in refrigerated rooms[15], the co-crystals adaptability was investigated performing additional release analyses at 4°C (Fig. 27, right column). As expected, at these conditions the active molecule release was significantly lower both for pure EOCs and for co-crystals with respect to the results observed at 30°C.

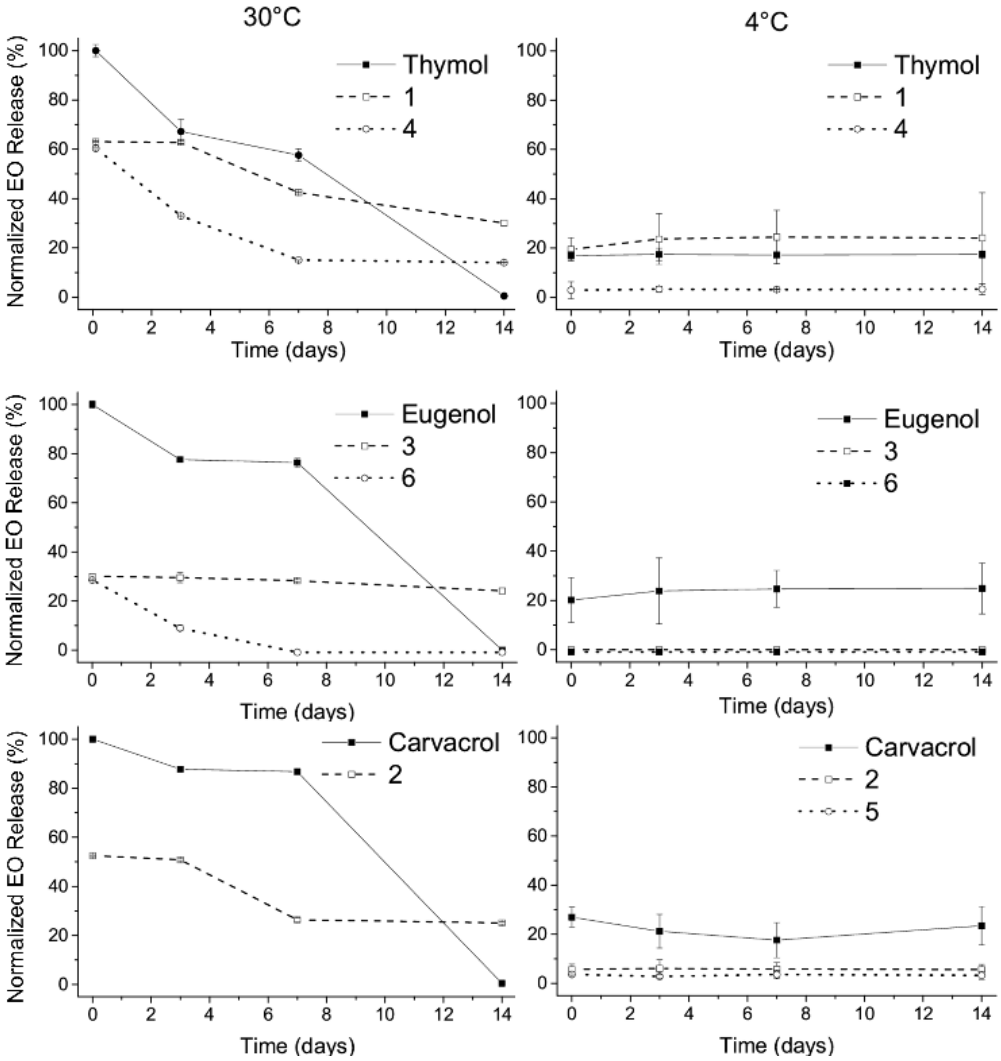

Figure 27. EOCs release profile from the pure substance (plain line) and from co-crystals (dashed and dotted lines) at 30°C (left) and 4°C (right). Release values were normalized with the acute release of EOC from the pure substance (i.e. after 5 minutes at 30°C). EOC-release of **5** was not tested at 30 °C because of its low melting temperature.

Furthermore, the release profile changed dramatically: the GC response smoothly decayed with respect to 30°C, thus suggesting an important

improvement in the use of these materials as food preservative in the refrigerated rooms.

WATER SOLUBILITY

Terpenes and terpenoids have a strong hydrophobic behavior which makes them inadequate for direct application on the plants. The increase of water solubility can then be essential for agronomical applications. Solubility in water of **1a-6** was tested at the standard concentration of 20 g/L which is the typical concentration of pesticides used for open field applications. Results evidenced that most of the co-crystals preserve the hydrophobic character of the pure EOC (**1a**, **2**, **3**, **4**; Table 10), with the exception of **5** and **6** for which an increased water solubility was observed.

3.3.3 ANTIBACTERIAL AND ANTIFUNGAL ACTIVITY

The antimicrobial activity of co-crystals **1a-6** and of the pure EOCs and coformers was tested by disk diffusion assay against six bacterial and three fungal species. The pathogenic species were systematically distant (i.e. belonging to different genera, therefore genetically very different) and able to attack different host plants causing various symptoms and economic losses[16]. All microbial species resulted sensitive to THY, CAR and EUG even though at different rate, as proved by statistical analysis. Kruskal-Wallis ANOVA results showed significant differences in the inhibitory effect on the microbial growth within each treatment combination: EOC, corresponding co-crystal, coformer and SDW (Sterilized Distilled Water as control) (Table 11).

		Treatment combination					
		THY, **1a**, PHE, SDW	CAR, **2**, PHE, SDW	EUG, **3**, PHE, SDW	THY, **4**, HMT, SDW	CAR, **5**, HMT, SDW	EUG, **6**, HMT, SDW
		$\chi^2(p)$					
		Bacteria					
Microorganisms	At	9.5*	10.6*	9.6*	10.6*	10.7*	10.6*
	Ba	10.5*	10.6*	10.6*	10.6*	10.7*	10.7*
	Cmm	11.7**	11.4**	11.2*	11.3**	11.2*	10.3*
	Pst	10.8*	10.4*	10.7*	11.0*	10.6*	10.7*
	Rf	10.7*	10.6*	9.9*	10.8*	10.6*	10.6*
	Xap	9.5*	10.4*	9.6*	10.5*	11.6*	10.7*
		Fungi					
	Aa	10.8*	10.5*	9.6*	11.0*	10.6*	10.7*
	Fol	10.8*	10.7*	9.8*	9.5*	10.7*	10.6*
	Pu	10.6*	8.9*	9.6*	10.7*	9.6*	9.7*

Table 11. Statistical results of the Kruskal-Wallis test examining variations in the antimicrobial effect of EOC, co-crystal, molecular coformer and SDW within each of the six different treatment combinations (d.f.=3; N° samples=12; p-value: * $p<0.05$ and ** $p<0.01$).

In fact, pure EOCs and co-crystals showed generally higher antimicrobial activity with respect to PHE and HMT, which displayed a very low bioactivity against the microorganisms under investigation. In particular, *Pst* resulted the less sensitive bacterium whereas *Cmm* and the fungus *Pu* were strongly inhibited by the activity of the three EOCs.

Results of the antibacterial and antifungal activity for thymol-based co-crystals are detailed in Table 12 (A and B).

A

Pathogen	SDW	TH_{HMT}	**1a** TH:PH	PH
			Bacteria	
At	0 a	1.86±0.08 b C	1.86±0.07 b B	0 a A
Ba	0 a	1.81±0.09 c C	2.28±0.07 d C	0.78±0.02 b C
Cmm	0 a	4.5±0 c D	4.5±0 c D	0.59±0.07 b C
Pst	0 a	0.34±0.04 b A	0.47±0.06 c A	0 a A
Rf	0 a	1.46±0.04 c B	1.75±0 d B	0.30±0.03 b B
Xap	0 a	2.02±0.24 b B	1.88±0.08 b B	0 a A
			Fungi	
Aa	0 a	4.5±0 c B	4.5±0 c B	1.34±0.08 b B
Fol	0 a	2.7±0.17 d A	2.0±0 c A	0.08±0 b A
Pu	0 a	6.33±0.08 d C	5.42±0.3 c C	2.4±0.15 b C

B

Pathogen	SDW	TH_{HMT}	**4** TH:HMT	HMT
			Bacteria	
At	0 a	1.86±0.08 c C	2.92±0.08 d C	0.49±0.01 b C
Ba	0 a	1.81±0.09 b C	2.58±0.27 c C	0 a A
Cmm	0 a	4.5±0 c D	4.5±0 c D	0.08±0.03 b B
Pst	0 a	0.34±0.04 b A	0.47±0.05 c A	0 a A
Rf	0 a	1.46±0.04 c B	1.75±0 d B	0.11±0.01 b B
Xap	0 a	2.02±0.24 b C	2.6±0.05 c C	0 a A
			Fungi	
Aa	0 a	4.5±0 b B	4.5±0 b B	0 a A
Fol	0 a	2.7±0.17 b A	3±0.76 c A	0 a A
Pu	0 a	6.33±0.08 c C	7±0 d C	2.4±0.06 b B

Table 12. Inhibitory effect of TH_{HMT}, TH:PH, PH (**A**) and of TH_{HMT}, TH:HMT, HMT (**B**) on the bacterial and fungal growth. Different letters indicate significant differences (p<0.05) by Mann-Whitney U Test: lowercase letters refer to the analysis between different treatments (d.f.=3, N° samples=12); upper case letters refer to the analysis within each single treatment between different species of bacteria (d.f.=5, N° samples=18-20) and fungi (d.f.=2, N° samples=9).

1a showed higher inhibitory effect on the growth of *Ba, Pst, Rf* than THY, and lower antimicrobial activity against *Fol* and *Pu*. No significant differences in the antimicrobial effect were observed between THY and **1a** against *At, Cmm, Xap* and *Aa.* **4** showed the highest inhibitory effect against *At, Ba, Pst, Rf, Xap, Fol* and *Pu*, whereas no significant differences in the antimicrobial activity were observed between THY and **4** against *Cmm* and *Aa*.

Regarding CAR (Table 13), **2** and **5** resulted significantly sensitive to the effect of the coformer: in fact, taking the performances of the single active component (CAR) as a reference, **2** showed a drop of 28-33% with respect to bacteria and fungi, whereas **5** showed an improvement of 10-44% in the antibacterial and antifungal effect. Specifically, **2** showed lower antimicrobial activity than CAR against *At, Ba, Cmm, Rf, Aa*, and *Fol*, whereas no significant differences were observed for *Pst, Xap* and *Pu*. **5** showed a stronger inhibiting activity than CAR against all the microorganisms with the exceptions of *Fol* (Fig.28).

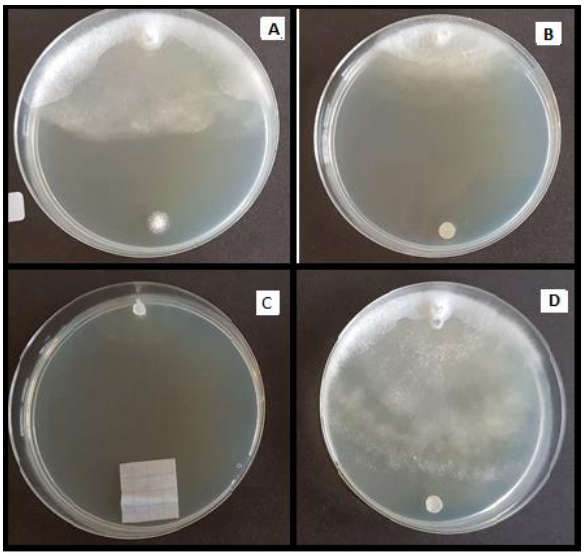

Figure 28. Inhibitory effect of HMT (A), CAR (B), HMT-CAR (C) and SDW (D) on the growth of the fungus *Pu.*

A

Pathogen	SDW	CAR_{HMT}	**2** CAR:PH	PH
			$\chi^2(p)$	
			Bacteria	
At	0 a	2.55±0.10 c D	1.78±0.12 b C	0 a A
Ba	0 a	2.27±0.03 d C	1.68±0.19 c C	0.78±0.02 b C
Cmm	0 a	2.65±0.23 d D	1.77±0.15 c C	0.59±0.07 b C
Pst	0 a	0.21±0.05 b A	0.25±0.02 b A	0 a A
Rf	0 a	2.60±0.10 d D	1.85±0.05 c C	0.30±0.03 b B
Xap	0 a	0.99±0.03 b B	0.86±0.07 b B	0 a A
	Fungi			
Aa	0 a	2.78±0.10 b B	1.95±0.23 c	1.34±0.08 b B
Fol	0 a	2.42±0.07 d C	2.02±0.11 c	0.08±0 b A
Pu	0 a	4.15±0.03 c B	4.17±0.43 c	2.40±0.15 b C

B

Pathogen	SDW	CAR_{HMT}	**5** CAR:HMT	HMT
			Bacteria	
At	0 a	2.55±0.10 c D	4.50±0 d D	0.49±0.01 b C
Ba	0 a	2.27±0.03 b C	3.10±0.03 c B	0 a A
Cmm	0 a	2.65±0.23 c D	4.50±0 d D	0.08±0.03 b B
Pst	0 a	0.21±0.05 b A	0.29±0.04 c A	0 a A
Rf	0 a	2.60±0.10 c D	3.78±0.03 d C	0.11±0.01 b B
Xap	0 a	0.99±0.03 b B	3.68±0.03 c C	0 a A
			Fungi	
Aa	0 a	2.78±0.10 b B	3.12±0.07 c B	0 a A
Fol	0 a	2.42±0.07 c C	2.15±0.03 b A	0 a A
Pu	0 a	4.15±0.03 c B	5.03±0.13 d C	2.40±0.06 b B

Table 13. Inhibitory effect of CAR_{HMT}, CAR:PHE, PHE (**A**) and of CAR_{HMT}, CAR:HMT, HMT (**B**) on the bacterial and fungal growth. Different letters indicate significant differences (p<0.05) by Mann-Whitney U Test: lowercase letters refer to the analysis between different treatments (d.f.=3, N° samples=12); upper case letters refer to the analysis within each single treatment between different species of bacteria (d.f.=5, N° samples=18-20) and fungi (d.f.=2, N° samples=9).

3 and EUG did not show significant differences in the antimicrobial activity against all the microorganisms with the exceptions of *Ba* and *Pu* that were

more sensitive to **3** and EUG respectively (Table 14; A). **6** showed the strongest activity against *At, Ba, Pst, Rf, Aa,* and *Fol*, whereas *Pu* was more sensitive to EUG. No significant differences were detected for *Cmm,* and *Xap* (Table 14; B).

A

Pathogen	SDW	EUG_{HMT}	**3** EUG:PH	PH
			Bacteria	
At	0 a	1.18±0.10 b B	1.28±0.03 b C	0 a A
Ba	0 a	0.88±0.01 b B	1.87±0.09 c E	0.78±0.02 b D
Cmm	0 a	1.52±0.02 c C	1.43±0.04 c D	0.59±0.07 b C
Pst	0 a	0.47±0.02 b A	0.58±0.03 b A	0 a A
Rf	0 a	1.02+0.02 c B	1.10±0.06 c B	0.30±0.03 b B
Xap	0 a	0.98±0.02 b B	1.02±0.06 b B	0 a A
			Fungi	
Aa	0 a	2.19±0.01 c B	2.09±0.2 c B	1.34±0.08 b B
Fol	0 a	1.65±0.01 c A	1.77±0.08 c A	0.08±0 b A
Pu	0 a	5.63±0.13 d C	4.42±0.3 c C	2.4±0.15 b C

B

Pathogen	SDW	EUG_{HMT}	**6** EUG:HMT	HMT
			Bacteria	
At	0 a	1.18±0.10 c B	1.89±0.02 d C	0.49±0.01 b C
Ba	0 a	0.88±0.01 b B	1.42±0.09 c BC	0 a A
Cmm	0 a	1.52±0.02 c C	1.67±0.34 c C	0.08±0.03 a B
Pst	0 a	0.47±0.02 b A	0.78±0.02 c A	0 a A
Rf	0 a	1.02+0.02 b B	1.19±0.04 c B	0.11±0.01 a B
Xap	0 a	0.98±0.02 b B	1.23±0.04 b B	0 a A
			Fungi	
Aa	0 a	2.19±0.01 b B	2.42±0.03 c A	0 a A
Fol	0 a	1.65±0.01 b A	2.14±0.04 c A	0 a A
Pu	0 a	5.63±0.13 d C	4.5±0 c B	2.4±0.06 b B

Table 14. Inhibitory effect of EUG_{HMT}, EUG:PH, PH (**A**) and of EUG_{HMT}, EUG:HMT, HMT (**B**) on the bacterial and fungal growth. Different letters indicate significant differences (p<0.05) by Mann-Whitney U Test: lowercase letters refer to the analysis between different treatments (d.f.=3, N° samples=12); upper case letters refer to the analysis within each single treatment between different species of bacteria (d.f.=5, N° samples=18-20) and fungi (d.f.=2, N° samples=9).

In sum, statistically significant improvements of antimicrobial effects were observed in 44% (24 over 54) of the treatments involving cocrystals, 20% (11 over 54) of treatments involving pure EOCs whereas no significant variations in inhibition of microbial growth among cocrystals and EOCs were detected in 35% (19 over 54) of the cases under investigation (about 33%). Furthermore, it has to be pointed out that inhibitory effects on microbial growth of **1a**, **2** and **3** might be underestimated since all tests were normalized to the amount of EOCs in HMT-based cocrystals which are stoichiometrically richer in EOCs (Table 9). Further studies are required to assess the efficacy of the three co-crystals *in vivo* against plant microorganisms having different ecology and mechanisms of infection.

3.4 CONCLUSIONS

In conventional agriculture the use of essential oil constituents is hampered by physical properties, such as their poor water solubility and the characteristic high volatility, which strongly affects the long-term efficacy of these compounds. Co-crystallization was then experimented to extend the range of applicability of EOCs. Following the philosophy of a more sustainable approach, a mechanochemical solvent-free synthesis was preferred to standard procedure. A set of six co-crystals based on thymol, carvacrol and eugenol was synthesized, and an in-depth structural characterization was performed. Water solubility, EOCs release and bioactivity were also determined and results showed an increase of the water solubility for HMT-CAR and HMT-EUG, whilst the other co-crystals preserved their hydrophobic character. A more controlled EOCs release was observed for co-crystals with

respect to the release profiles of pure substances, pointing out the crucial role played by co-crystallization in the long-term release of the bioactive molecule. Finally, the antimicrobial properties of co-crystals were tested against six bacteria and three fungi. Overall co-crystals' performances were comparable to those shown by the pure EOCs, but in some cases a synergic effect ascribed to the EOC/coformer matching was observed, thus allowing an extension of the antimicrobial spectrum of activity.

3.5 REFERENCES

[1] De, A., Bose, R., Kumar, A., & Mozumdar, S. (2014). Worldwide pesticide use. In *Targeted delivery of pesticides using biodegradable polymeric nanoparticles* (pp. 5-6). Springer, New Delhi.

[2] Martínez-Ballesta, M. C., López-Pérez, L., Muries, B., Muñoz-Azcarate, O., & Carvajal, M. (2009). Climate change and plant water balance: the role of aquaporins–a review. In *Climate Change, Intercropping, Pest Control and Beneficial Microorganisms* (pp. 71-89). Springer, Dordrecht.

[3] Singh, N. S., Sharma, R., Parween, T., & Patanjali, P. K. (2018). Pesticide contamination and human health risk factor. In *Modern Age Environmental Problems and their Remediation* (pp. 49-68). Springer, Cham.

[4] Bakkali, F., Averbeck, S., Averbeck, D., & Idaomar, M. (2008). Biological effects of essential oils–a review. *Food and chemical toxicology*, *46*(2), 446-475.

[5] Isman, M. B., & Miresmailli, S. (2011). Plant essential oils as repellents and deterrents to agricultural pests. In *Recent developments in invertebrate repellents* (pp. 67-77). American Chemical Society.

[6] Aakery, C. B., & Salmon, D. J. (2005). Building co-crystals with molecular sense and supramolecular sensibility.

[7] Javoor, M. G., Mondal, P. K., & Chopra, D. (2017). Cocrystals: a review of recent trends in pharmaceutical and material science applications. *Material Science Research India*, *14*(1), 09-18.

[8] Aakeröy, C. B., Wijethunga, T. K., Benton, J., & Desper, J. (2015). Stabilizing volatile liquid chemicals using co-crystallization. *Chemical Communications*, *51*(12), 2425-2428.

[9] Bacchi, A., Capucci, D., Giannetto, M., Mattarozzi, M., Pelagatti, P., Rodriguez-Hornedo, N., ... & Sala, A. (2016). Turning Liquid Propofol into Solid (without Freezing It): Thermodynamic Characterization of Pharmaceutical Cocrystals Built with a Liquid Drug. *Crystal Growth & Design*, *16*(11), 6547-6555.

[10] Bassanetti, I., Carcelli, M., Buschini, A., Montalbano, S., Leonardi, G., Pelagatti, P., ... & Rogolino, D. (2017). Investigation of antibacterial activity of new classes of essential oils derivatives. *Food Control*, *73*, 606-612.

[11] James, S. L., & Friščić, T. (2013). Mechanochemistry. *Chemical Society Reviews*, *42*(18), 7494-7496.

[12] Braga, D., Maini, L., & Grepioni, F. (2013). Mechanochemical preparation of co-crystals. *Chemical Society Reviews*, *42*(18), 7638-7648.

[13] OECD, T. (1995). Test No. 105: Water Solubility.

[14] Kuorwel, K. K., Cran, M. J., Sonneveld, K., Miltz, J., & Bigger, S. W. (2011). Essential oils and their principal constituents as antimicrobial agents for synthetic packaging films. *Journal of Food Science*, *76*(9), R164-R177.

[15] Jacob, A. G., Uduma, A. U., Adesoji, A. G. (2017). Potatoes Sprout Suppressant Activity of Essential Oils of Monodora Tenuifolia, Cymbopogon Citratus and Ocimum Gratissimum. *Chem. Res. J.*, *2* (3), 214–218.

[16] Savary, S., Ficke, A., Aubertot, J. N., & Hollier, C. (2012). Crop losses due to diseases and their implications for global food production losses and food security.

LIST OF ACRONYMS AND ABBREVIATIONS

SECTION 1

CISM: Centro di servizi di Spettrometria di Massa

Cv: cultivar

DLS: Dynamic Light Scattering

DOPC: 1,2-Dioleyl-sn-glycero-3-phosphocholine

DOPE: 1,2-dioleyl-sn-glycero-3-phosphoethanolamine

IAA: Indole-3-acetic acid

IBA: Indole-3-butyric acid

NAA: 1-naphtaleneacetic acid

OM: Olive Medium

OMP: Olive Mill Pomace

OP: Olive Pomace

PC: same as DOPC

PdI: Polidispesity index

PE: same as DOPE

SAXS: Small Angle X-ray Scattering

SP: Standard Procedure

T: treatment

ZP: Zeta Potential

SECTION 2

BLS: Bacterial Leaf Spot

DAGRI: Department of Agriculture, Food, Environment and Forestry

DLS: Dynamic Light Scattering

DOPE: 1,2-dioleyl-sn-glycero-3-phosphoethanolamine

FAMEs: Fatty Acids Methyl Esters

GC-MS: Gas Chromatography-Mass Spectrometry

MIC: Minimum Inhibitory Concentration

N: *Nannochloropsis* sp.

NAG: Nutrient Glucose Agar

NB: Non-loaded *Nannochloropsis*-derived nanovectors

NT: Thymol-loaded *Nannochloropsis*-derived nanovectors

NVs: Nanovectors

OD: Optical Density

PDA: Potato Dextrose Agar

Pst: *Pseudomonas syringe* pv. *tomato*

S100 B: Soybean phosphatidylcholine non-loaded nanovectors

S100 T: Soybean phosphatidylcholine thymol-loaded nanovectors

S100: Soybean phosphatidylcholine

SAXS: Small Angle X-ray Scattering

TAGs: Triacylglycerides

Xcv: *Xanthomonas campestris* pv. *vesicatoria*

SECTION 3

Aa: *Alternaria alternata*

Ba: *Bacillus amyloliquefaciens* (Ba M123)

CAR: Carvacrol

Cmm: *Clavibacter michiganensis* subsp. *Michiganensis*

EOC(s): Essential Oil Constituent(s)

EUG: Eugenol

Fol: *Fusarium oxysporum* f.sp. *lycopersici*

HBP: Hydrogen Bond Propensity

HMT: Hexamethylenetetramine

IPSP-CNR: Istituto per la Protezione Sostenibile delle Piante – Consiglio Nazionale delle Ricerche

MC score: Multi-component score

NAG: Nutrient Glucose Agar

OD: Optical Density

OECD: Organization for Economic Co-operation and Development

PDA: Potato Dextrose Agar

PHE: Phenazine

Pst: *Pseudomonas syringae* pv. *tomato* (Pst 50)

Pu: *Pythium ultimum*

Rf: *Rhodococcus fascians* (Rf LMG 3605)

RIB: Riboflavin

SDW: Sterile Distilled Water

SS: Saline Solution

THE: Theobromine

THY: Thymol

VAN: Vanillin

Xap: *Xanthomonas arboricola* pv. *pruni* (Xap Lc)

PUBBLICATIONS

Mazzeo, P. P., Carraro, C., Monica, A., Capucci, D., Pelagatti, P., Bianchi, F., ... & Menicucci, F. (2019). Designing a palette of Cocrystals based on Essential Oil constituents for agricultural applications. *ACS Sustainable Chemistry & Engineering*. *7*(21), 17929-17940.

Bonciu, E., Firbas, P., Fontanetti, C. S., Wusheng, J., Karaismailoğlu, M. C., Liu, D., Menicucci, F., ... & Schiff, S. (2018). An evaluation for the standardization of the Allium cepa test as cytotoxicity and genotoxicity assay. *Caryologia*, *71*(3), 191-209.

Clemente, I., Menicucci, F., Colzi, I., Sbraci, L., Benelli, C., Giordano, C., ... & Petruccelli, R. (2018). Unconventional and sustainable nanovectors for phytohormone delivery: insights on Olea europaea. *ACS Sustainable Chemistry & Engineering*, *6*(11), 15022-15031.

Alessio Papini, Cristina Gonnelli, Corrado Tani, Pietro Di Falco, Giovanna Wolswijk, Ugo Santosuosso, Caterina Nuccio, Silvia Schiff, Luigi Lazzara, Felicia Menicucci, Mattia Belli, Tiruha Habte Karssa and Raffaello Ballini (2018) Autophagy Induced by Heavy Metal and Starvation Stress in Microalgae. Phytomorphology 68(1&2): 7-12.